Advancement of the detection of individual Alzheimer's amyloid-β oligomers in biological samples

Inaugural-Dissertation

zur Erlangung des Doktorgrades

der Mathematisch-Naturwissenschaftlichen Fakultät

der Heinrich-Heine-Universität Düsseldorf

vorgelegt von

Kun Wang

aus Shiyan, China

Düsseldorf, November 2014

aus dem Institut für Physikalische Biologie

der Heinrich-Heine-Universität Düsseldorf

Gedruckt mit der Genehmigung der

Mathematisch-Naturwissenschaftlichen Fakultät der

Heinrich-Heine-Universität Düsseldorf

Referent: Prof. Dr. rer. nat. Dieter Willbold

Korreferent: Prof. Dr. rer. nat. Georg Groth

Tag der mündlichen Prüfung:

Table of Contents

List of figures

List of tables

1 Introduction

1.1 Alzheimer's disease

Alzheimer's disease (AD) is a progressive neurodegenerative disease which was first described in 1907 (Alzheimer, 1907). The majority of diagnosed AD cases lies in the age group above 65, which reflects the correlation of ageing and the disease (Brookmeyer et al., 1998). 26.6 million people worldwide suffered from AD in 2006 (Brookmeyer et al., 2007). It is estimated that over 100 million patients will develop AD by 2050 (Wimo and Prince, 2011). The fact that there is so far no cure for AD together with the degenerative manner of the disease has put mounting pressure on the health system as well as the society.

AD usually progresses through several stages. The early, preclinical stage shows no symptoms; the middle stage of mild cognitive impairment (MCI); and the final stage of Alzheimer's dementia (Burns and Iliffe, 2009). AD shows common symptoms of short-term memory loss at its onset. As the disease progresses, further symptoms such as long-term memory loss, trouble with language and loss of bodily functions develop, which ultimately leads to death (Bird, 1993). The development of AD is distinct from one individual to another, which can progress undiagnosed for years. The average life expectancy after diagnosis is approximately seven years (Molsa et al., 1986).

In the brain of AD patients, amyloid plaques and neurofibrillary tangles (NFTs) are observed, together with the atrophy of the affected regions caused by the loss of neurons and synapses (Wenk, 2003). Amyloid plaques are dense deposits composed of amyloid-β (Aβ) peptide and extracellular material (Iwatsubo et al., 1994), while the neurofibrillary tangles are intracellular aggregates of hyperphosphorylated tau protein (Grundke-Iqbal et al., 1986).

Tau is a protein concentrating in the axon. Tau functions in stabilizing the microtubules which are part of the cytoskeleton. These microtubules guide the intracellular transportation of nutrients and other molecules. Aβ peptide is a fragment of integral membrane protein called amyloid precursor protein (APP). APP functions

in neuronal growth, survival and post-injury repair. Aβ is derived from sequential cleavage of APP (Kang et al., 1987). The distribution of APP concentrates in the synapses of neurons (Priller et al., 2006).

Though 5% to 10% of all AD cases, known as familial AD, can be attributed to the genetic background, the cause for the remaining majority AD cases, also referred to as sporadic AD, is still unidentified (Goedert et al., 1994). There are several different hypotheses for the cause of the disease. The tau hypothesis proposes the tau protein malfunction as the fundamental cause of the disease. Normal tau protein is phosphorylated on approximately 30 sites. According to tau hypothesis, the hyperphosphorylated tau protein associates with each other, which leads to the formation of neurofibrillary tangles. Moreover, hyperphosphorylated tau causes the disassembly of microtubules by excluding normal tau and other microtubule-associated proteins (Hernandez and Avila, 2007). On the other hand, the amyloid hypothesis proposes that the primary driving force of AD pathogenesis is the Aβ deposition in the brain. The imbalance between Aβ production and Aβ clearance triggers a series of events including formation of neurofibrillary tangles as well as neuronal dysfunction and death (Hardy and Selkoe, 2002; Small and Duff, 2008). However, there are studies suggesting that tau hyperphosphorylation and Aβ accumulation might be independent pathophysiological processes (Duyckaerts, 2011; Small and Duff, 2008).

1.2 Amyloid-β and amyloidogenesis

Aβ peptide was first sequenced in a study on the cerebrovascular amyloid fibril protein (Glenner and Wong, 1984b). Later Aβ peptide was isolated and purified from amyloid plaques with its size determined as about 4.5 kDa (Masters et al., 1985). Aβ peptide is a natural metabolic product. Figure 1-1 shows that a set of isoforms of Aβ peptide comprising 38 to 43 amino acids are generated through a sequential cleavage of APP by β- and γ-secretase (Gandy, 2005).
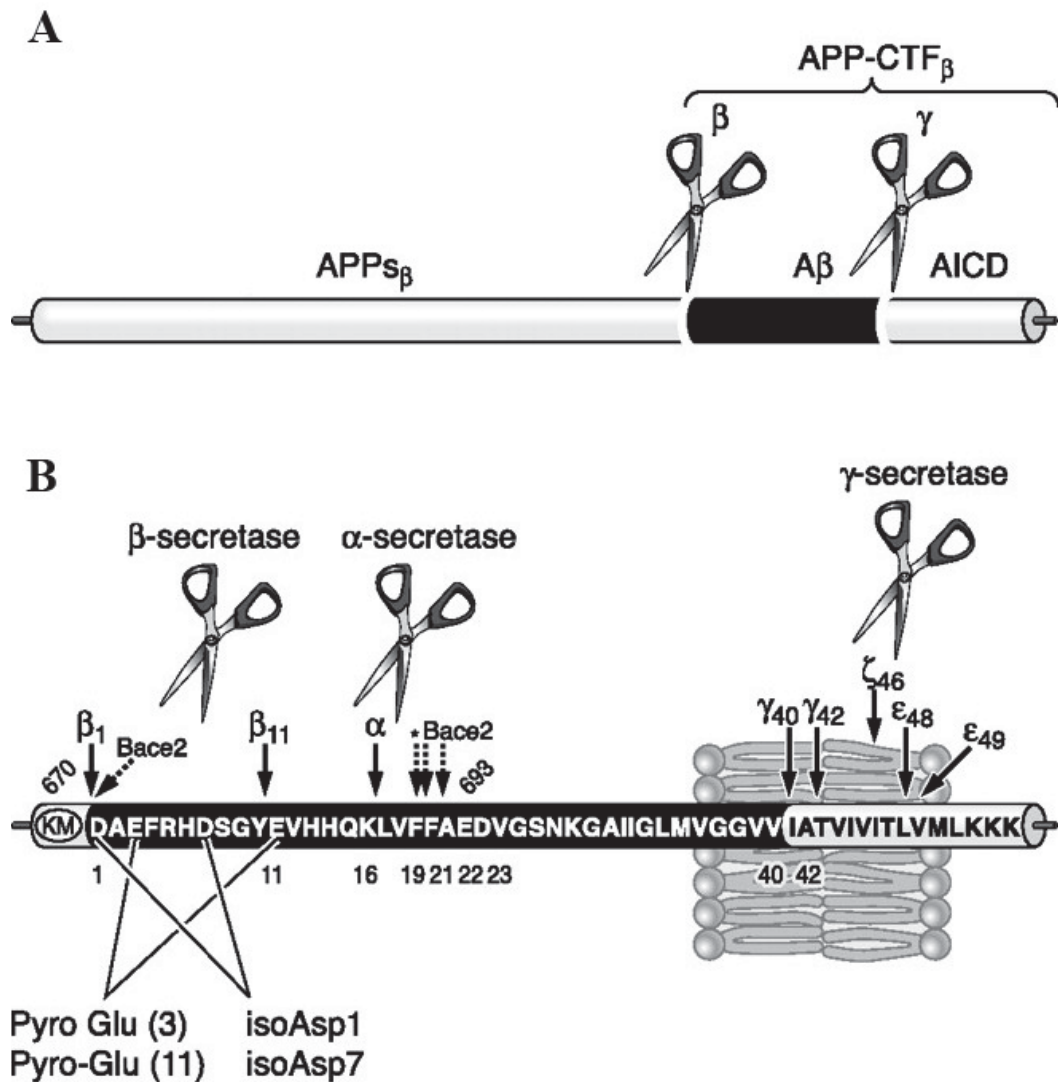
Figure 1-1: The proteolysis of the amyloid precursor protein (APP)

APP is an integral membrane protein with extracellular N-terminal tail. Aβ is generated when APP is processed in the β-secretase pathway. (A) Cleavage by β-secretase yields APPsβ and APP-C-terminal fragment (CTF) β. Further cleavage by γ-secretase generates Aβ and amyloid precursor protein intracellular domain (AICD). Cleavage sites of β-, and γ-secretase are indicated. (B) The amino acid sequence of Aβ is demonstrated in the one-letter code. Aβ1-40 and Aβ1-42 are the products of cleavage by γ-secretase at different sites. The different cleavage sites by β-, α-, and γ-secretases are indicated. The amino acid residues which are modified by pyroglutamate or isoaspartyl are also indicated. (scheme modified from De Strooper, 2010).

Aβ peptide distributes in different body fluids such as cerebrospinal fluid (CSF) and plasma (Seubert et al., 1992; Shoji et al., 1992). So far the physiological role of Aβ is poorly understood. However, some studies suggest certain potential functions of Aβ.

Aβ could be involved in the activation of kinase enzymes (Tabaton et al., 2010), regulation of cholesterol transport (Igbavboa et al., 2009) and protection against oxidative stress (Baruch-Suchodolsky and Fischer, 2009). In another study Aβ also showed neurotoxic effect of inducing neuronal cell death (Nakagawa et al., 2000).

Various isoforms of Aβ have been detected in the brains of AD patients. The most abundant isoform is Aβ1-40 (LaFerla et al., 2007), but Aβ1-42 has found to be the predominant isoform in cerebral plaques (Younkin, 1998). In comparison with Aβ1-40, the two additional amino acids (isoleucine and alanine) at the C-terminus of Aβ1-42 make it more hydrophobic and cause a greater tendency to aggregate (Wong et al., 2002). In a study combining simulation and nuclear magnetic resonance (NMR) measurement, the C-terminus of Aβ1-42 showed reduced structural flexibility compared to that of Aβ1-40 (Sgourakis et al., 2007). N-terminus truncated pyroglutamylated peptides AβpGlu3-42 and AβpGlu11-42 have been identified in the brains as well as in the CSF of AD patients (Lewczuk et al., 2003). The pyroglutamate modification on the N-terminus changes the secondary structure and the hydrophobicity of Aβ peptide, therefore enhance its amyloidogenicity (Schilling et al., 2011).

The self-propagation of Aβ aggregates has been observed from inoculation experiments on animal (Baker et al., 1993). It took more time to observe that the deposition of Aβ could be induced by seeding exogenous tissue into transgenic animal (Jucker, 2010). This showed similar infection mechanism to prion. More findings showed the similarity between the amyloidogenesis in Alzheimer's disease and Parkinson's disease and the pathogenesis of the prion diseases (Braak et al., 2003; Thal et al., 2002), in which the infectious isoform of prion protein (PrP^{Sc}) induces the conformation change of the normal form of prion protein (PrP^{C}), turning them into infectious isoform so that they can form aggregates (Caughey et al., 2009).

So far the molecular mechanism of the formation of amyloid is not fully understood. There are several intermediate forms such as oligomers and protofibrils involved in the amyloidogenesis (Figure 1-2). Current studies suggest that the conformational transformation, in which unstructured, α-helix, and β-strand elements convert into predominantly β-sheet/β-turn structures, is linked to toxicity (Bitan et al., 2003).
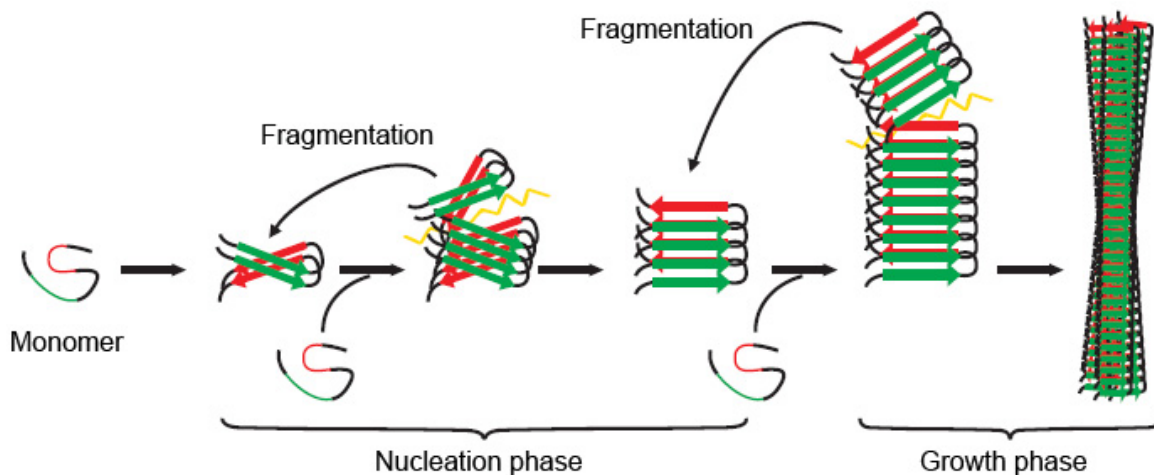
Figure 1-2: The model of amyloid protein aggregation

In general, the formation of amyloid begins with a seeding process in which the aggregating proteins form nuclei. This phase may include a series of intermediate states until the initial amyloid backbone takes shape. Through conformational conversion monomers or oligomers then bind to the amyloid seed. When the growing structure is no longer stable in its conformation, it breaks so that new amyloid seeds are generated and proliferate to form more amyloid. (scheme modified from Jucker and Walker, 2013)

1.3 Diagnosis and biomarkers of Alzheimer's disease

Alzheimer's disease is currently affecting the lives of millions, and due to the ageing societies increasing number of cases are expected. However, the only definitive diagnosis can only be made by the *post mortem* autopsy (Ballard et al., 2011). The current clinical diagnosis of AD depends largely on the mental status test, standard medical tests (blood and/or urine tests) and brain imaging (Jack et al., 2011). However, the pathophysiological process, which involves inflammation as well as neuronal damage, has already begun in the preclinical stage of AD (Price et al., 2009). Therefore reliable methods to detect AD pathology in the preclinical stage are essential for the early intervention and treatment of the disease.

The current efforts on early detection of AD are focused on biomarkers. A biomarker is defined as a parameter that can be used to measure biological or pathological processes. Some AD biomarkers have already shown to have the potential for clinical trials (Jack and Holtzman, 2013). One group of the biomarkers are characterized by

the Aβ accumulation: the CSF Aβ1-42 (Visser et al., 2009) and positron emission tomography (PET) amyloid imaging (Drzezga, 2010). Another group is featured by the neurodegeneration: the total (t-tau) and phosphorylated tau (p-tau) in CSF (Mattsson et al., 2009), atrophy measured by structural MRI (Dickerson and Wolk, 2012), and hypometabolism on fluorodeoxyglucose (FDG) PET (Jagust et al., 2010). Figure 1-3 shows a hypothetical model which has been proposed to illustrate relationship of the AD biomarkers to the longitudinal clinical symptoms (Jack et al., 2013).
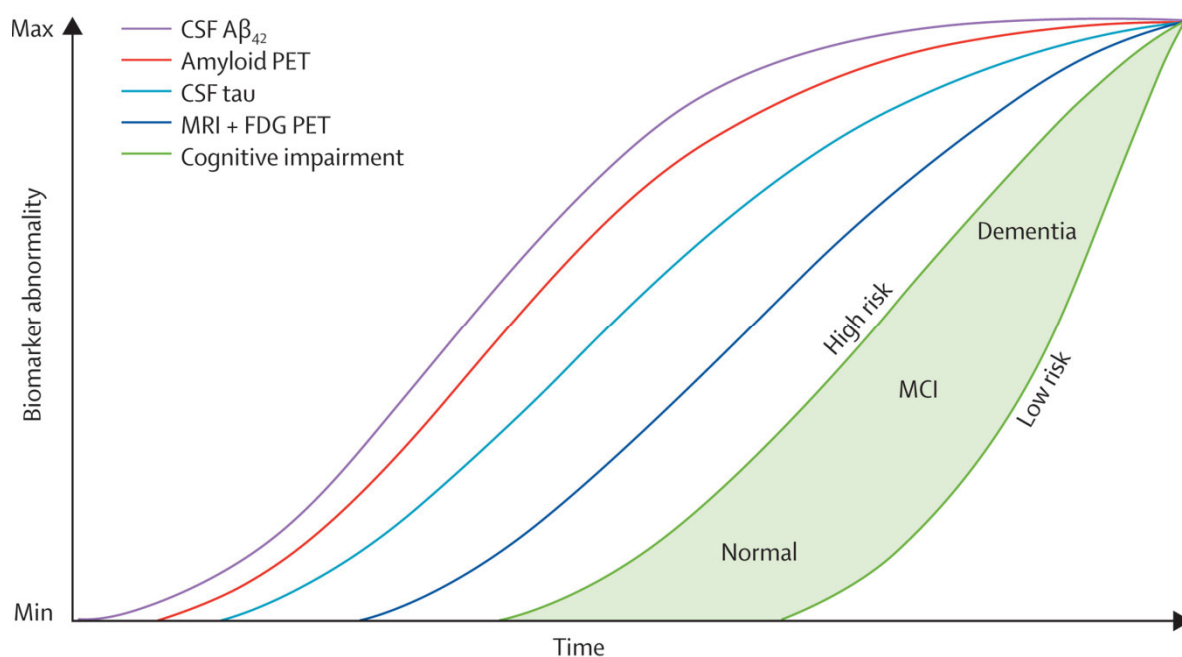
Figure 1-3: The model of AD biomarkers and AD pathology

CSF Aβ (purple line) and amyloid PET imaging (red line) show Aβ levels detected by different methods. CSF tau (light blue line) indicates CSF t-tau and CSF p-tau. Neurodegeneration is measured by FDG PET and structural MRI (dark blue line). Cognitive impairment is illustrated as a zone (light green-filled area) with low-risk and high-risk borders (green lines). The cognitive impairment curve shifting to the left indicates the cases which are at high risk of cognitive impairment caused by AD pathophysiology. By contrast, the cognitive impairment curve shifting to the right indicates those cases which are exposed to low risk of cognitive impairment caused by AD pathophysiology. (scheme modified from Jack et al., 2013)

As shown in Figure 1-3, the change in CSF Aβ1-42 level is ahead of all other biomarkers in the progression of the disease. The decreased CSF Aβ1-42 level could be related to the Aβ aggregation and deposition in the brain. And as reported by many studies, the soluble oligomeric species of Aβ induce neuronal damage and loss (Shankar et al., 2008). Thereby the soluble Aβ oligomers, not the Aβ monomers, have been proposed to account for the neurotoxicity (Glabe, 2006). Several techniques have been developed to detect Aβ oligomers, including immunoblotting (Tomic et al., 2009), enzyme-linked immunosorbent assay (ELISA) (LeVine, 2004) and a nanoparticle-based bio-barcode assay (Georganopoulou et al., 2005).

However, these techniques can only provide the information of the overall concentration of Aβ oligomers within the sample. The information of the shape, size and composition of the Aβ oligomers cannot be provided. A set of methods have been developed to obtain more detailed information of the Aβ oligomers on the single molecule level. One detection method of single Aβ aggregates was established using one-color fluorescence labeled Aβ peptide using fluorescence correlation spectroscopy (FCS) (Pitschke et al., 1998). Large Aβ1-42 binding particles (LAPs) in human CSF have been detected using confocal microscopy (Henkel et al., 2007). Another method combining flow cytometry and fluorescence resonance energy transfer (FRET) was used to examine the structures of Aβ oligomers and fibrils (Santos et al., 2007). Those studies revealed more comprehensive knowledge of Aβ oligomers on the single molecule level.

1.4 Detection of peptide aggregates using surface-based-fluorescence intensity distribution analysis

The method of single Aβ aggregates detection using FCS laid the foundation for the detection of single Aβ oligomer particles (Pitschke et al., 1998). The method was adopted to detect the single prion protein (PrP) particles in the brain tissue of prion-infected cattle and sheep (Birkmann et al., 2006). The introduction of two detection antibodies each with a distinct type of fluorescence dye made the PrP aggregates highly fluorescent. The FCS measurement was applied in a dual-color mode, for which the evaluation procedure called fluorescence intensity distribution analysis

(FIDA) was applied. There were several advantages of the FCS, such as the low amount of samples required for the measurement as well as the ability to determine the diffusion time and the molecular weight of the fluorescence molecules. However, there were also some disadvantages. Firstly, big PrP aggregates showed very slow or even undetectable diffusion. Moreover, due to their insoluble nature they tend to sink to the bottom of the chip and cannot be detected anymore. Secondly, only a small part of the sample could be analyzed due to the very small detection volume compared to the whole sample volume.

Therefore a further improvement was introduced to overcome the above problems. In the experimental setup called surface-FIDA i.e. a previous format of the current sFIDA technique, PrP aggregates were immobilized to the glass surface by capture antibody which recognizes the PrP (Birkmann et al., 2007). The capture antibodies bound to the surface coated with poly-D-lysine (PDL) by non-covalent adhesion. The new approach increased the sensitivity of the assay, which made the counting of individual prion particles possible. PrP aggregates were also detected in the blood plasma samples through modifying the protocol by binding the capture antibodies covalently to the surface (Bannach et al., 2012). In a parallel development, sFIDA was also adapted to detect Aβ aggregates for AD diagnosis (Funke et al., 2007). Three antibodies were used in this assay, one of which was capture antibody and the other two were detection antibodies. The assay specifically detected Aβ oligomers and aggregates. As two of the three antibodies recognized overlapping epitopes, Aβ monomers were excluded by dual-color detection and cross-correlation analysis. The protocol was further optimized by using carboxylmethyl dextran (CMD) instead of poly-D-lysine as a spacer to bind the capture antibody covalently to the glass surface. The optimization reduced the fluorescence background. Moreover, a confocal microscope instead of FCS was used for measuring the fluorescence signals. The generated images made it possible to analyze not only cross-correlated pixels and their intensities, but also the shape and size of the particles (Wang-Dietrich et al., 2013). A scheme of the working setup of sFIDA is shown in Figure 1-4.
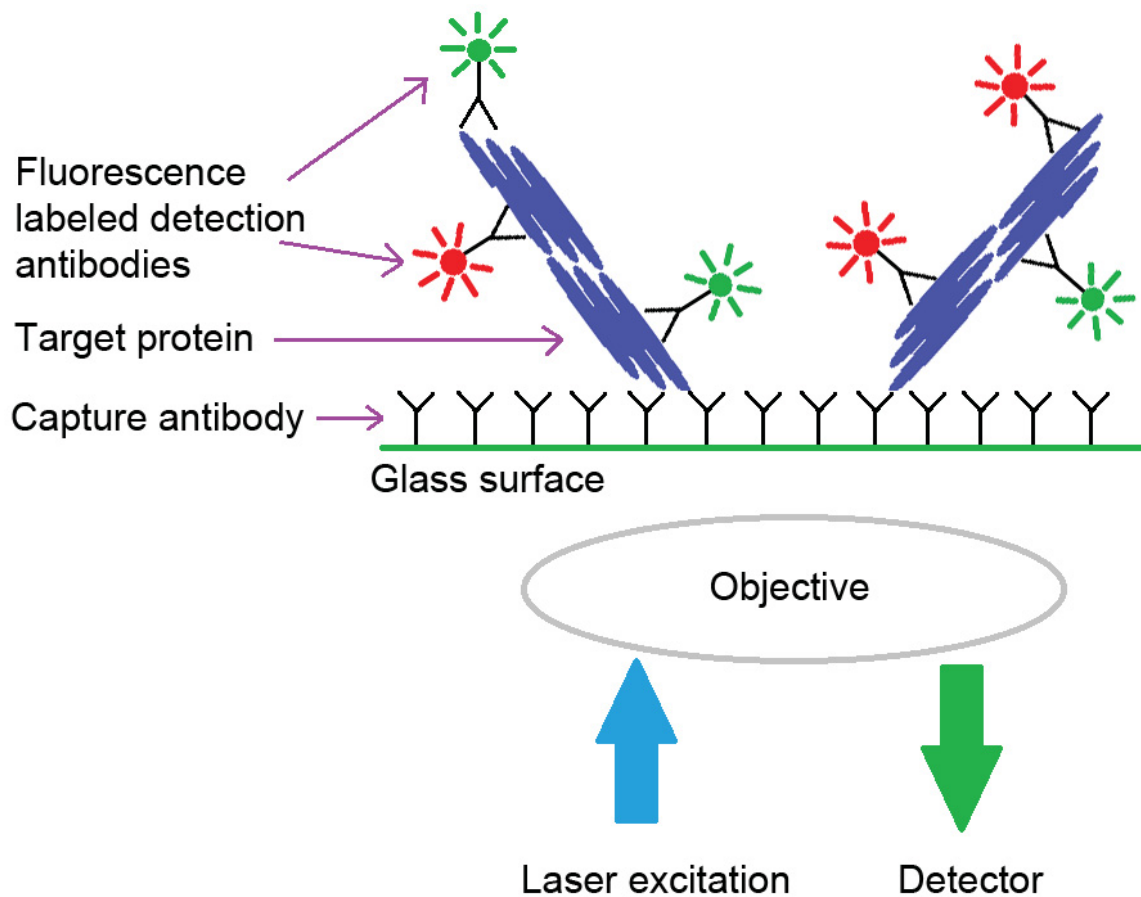
Figure 1-4: The setup of sFIDA using fluorescence microscopy

The glass surface is chemically modified so that the capture antibodies are immobilized on the surface. The target proteins in the samples are captured by the capture antibodies. The target proteins are then recognized by the two fluorescence labeled detection antibodies. The imaging is then achieved by the fluorescence microscopy.

1.5 Aim of this work

Playing a key role in the AD pathogenesis, Aβ has been used as an AD biomarker in various studies (Glenner and Wong, 1984a; Hardy and Selkoe, 2002). The establishment of sFIDA has enabled the detection of synthetic Aβ oligomer as well as the endogenous Aβ oligomer in human CSF samples (Funke et al., 2007; Wang-Dietrich et al., 2013). This work aims at measuring human CSF samples from various sources and establishing a robust platform to distinguish different types of samples (e.g. control, MCI and AD). One of the challenges faced by sFIDA has been the systemic variation which makes it difficult to compare one measurement with another. Trying to establish a reliable reference system for sFIDA, this work has explored the capability of multiple antigenic peptide (MAP) molecules as a reference standard. Another challenge is the quality control of the capture antibody coating. The quality such as homogeneity of the capture antibodies is crucial for the assay. Thus it is needed to establish a method to inspect the quality of the capture antibody. This work is supposed to optimize the sFIDA assay for more robust detection of Aβ oligomers in biological fluid samples.

2 Materials and methods

2.1 Materials

2.1.1 Chemicals

Table 2-1: List of chemicals

Chemical	Catalogue number, Company
2-Amino-2-hydroxymethyl-propane-1,3-diol-Hydrochloride (Tris-HCl)	857645, Sigma-Aldrich, Germany
Bovine serum albumin (BSA), fraction V	10735086001, Roche, Germany
Carboxymethyl dextran sodium salt (CMD)	86524, Sigma-Aldrich, Germany
Dimethyl sulfoxide (DMSO)	D5879, Sigma-Aldrich, Germany
Disodium phosphate (Na_2HPO_4)	4984.1, Carl Roth, Germany
Ethanolamine hydrochloride	E6133, Sigma-Aldrich, Germany
1,1,1,3,3,3-Hexafluor-2-propanol (HFIP)	105228, Sigma-Aldrich, Germany
Hydrochloride (HCl)	A0659, AppliChem, Germany
Monopotassium phosphate (KH_2PO_4)	3904.1, Carl Roth, Germany
N-(3-dimethyl-aminopropyl)-N'-ethylcarbodiimide hydrochloride (EDC)	03450, Sigma-Aldrich, Germany
N-hydroxysuccinimide (NHS)	130672, Sigma-Aldrich, Germany
Potassium chloride (KCl)	A3582, AppliChem, Germany
Sodium chloride (NaCl)	A3597, AppliChem, Germany
Sodium dodecyl sulfate (SDS)	CN30.2, Carl Roth, Germany
Sodium hydrogen carbonate ($NaHCO_3$)	6885.1, Carl Roth, Germany
Streptavidin	85878, Sigma-Aldrich, Germany
Toluene	108326, Merck, Germany
Tween-20	A4974, AppliChem, Germany

2.1.2 Buffers

The buffers are autoclaved for 20 min, 1.2 bar at 121 °C unless mentioned otherwise.

Table 2-2: List of buffers

Buffer	Ingredients
Phosphate buffered saline (PBS)	140 mM NaCl, 2.7 mM KCl, 10 mM Na_2HPO_4, 1.8 mM KH_2PO_4, pH 7.4
Tris-buffered saline (TBS)	25 mM Tris-HCl; 150 mM NaCl, 3 mM KCl, pH 7.4
TBS-Tween (TBST)	25 mM Tris-HCl; 150 mM NaCl, 3 mM KCl, pH 7.4, 0.1% (v/v) Tween-20

2.1.3 Antibodies

Table 2-3: List of Antibodies

Antibody	Ingredients
Alexa Fluor 488 monoclonal anti-Aβ, 6E10	Covance, Emeryville, California, USA
Monoclonal anti-Aβ, 6E10	Covance, Emeryville, California, USA
Monoclonal anti-Aβ, NAB228	Sigma-Aldrich, München, Germany
Monoclonal anti-Aβ, IC16	University of Duesseldorf Medical School

2.1.4 Peptides

Table 2-4: List of peptides

Peptide	Sequence	Company
Aβ1-42	CH_3CO-AIVVGGVMLGIIAGKNSGVDEAFFVLKQHHVE YGSDHRFEAD-NH_2	JPT, Germany
4MAP	CH_3CO-DAEFRHDSGYEDAEFRHDSGYEKDAEFRHDSG YEDAEFRHDSGYEKKWWK(biotin)-NH_2	JPT, Germany
8MAP	CH_3CO-DAEFRHDSGYEDAEFRHDSGYEKDAEFRHDSG YEDAEFRHDSGYEKDAEFRHDSGYEDAEFRHDSGYE KDAEFRHDSGYEDAEFRHDSGYEKKKKWK(biotin)-NH_2	Cambridge Peptides, UK

2.1.5 Human CSF samples

Human cerebrospinal fluid (CSF) samples, which derived from control and AD positive individuals, were purchased from BioChemed (Winchester, USA). The sample numbers are listed in Table 2-5.

Table 2-5: Table of CSF samples purchased from BioChemed

Control Sample No.	AD Sample No.
21-8	0367
27-5	365
27-7	378
31-6	4352
786	4367

13

Human CSF samples including control, MCI and AD subjects were kindly provided by Prof. Piotr Lewczuk, Universitätsklinikum Erlangen. The sample numbers and the corresponding Aβ1-42 concentration (pg/ml) are listed in Table 2-6.

Table 2-6: Table of CSF samples provided by Universitätsklinikum Erlangen

Control		MCI		AD	
Sample No.	Aβ1-42 [pg/ml]	Sample No.	Aβ1-42 [pg/ml]	Sample No.	Aβ1-42 [pg/ml]
006	909	057	641	047	594
009	1108	125	681	087	632
028	878	158	546	105	588
040	957	160	750	234	587
045	1995	191	614		
049	1580	239	733		
076	1451				
100	1419				
136	1915				

2.1.6 Kits

Table 2-7: List of kits

Kit (Catalog number)	Company
Alexa Fluor 488 Monoclonal Antibody Labeling Kit	Life Technologies, USA
Alexa Fluor 546 Monoclonal Antibody Labeling Kit	Life Technologies, USA
Alexa Fluor 633 Protein Labeling Kit (A20170)	Life Technologies, USA
Alexa Fluor 647 Monoclonal Antibody Labeling Kit	Life Technologies, USA
ATTO 488 (NHS-Ester)	ATTO-TEC, Germany
ATTO 647N (NHS-Ester)	ATTO-TEC, Germany

2.1.7 Plates

Custom-made 384-well glass microtiter plates were purchased from mikroglas chemtech (Mainz, Germany). The glass bottom is 0.17 mm thick and the round surface of each well has a diameter of 3.5 mm, making a surface area of about 9.6 mm^2. The depth of the well was 6.0 mm, giving a well volume of about 58 µl.

Custom-made 96-well glass microtiter plates were provided by the Zentralabteilung für Technologie (ZAT) at the Forschungszentrum Jülich. The plates with 96 holes were provided by ZAT. The glass bottom (Menzel-Gläser) is 0.17 mm thick and was attached to the plate with 96 holes by glue (UV Adhesive VERIFIX LV 740). The round surface of each well has a diameter of 3.5 mm, making a surface area of about 9.6 mm^2. The depth of the well was 5.5 mm, giving a well volume of about 53 µl.

Table 2-8: List of plates

Type	Company
96 Well glass microtiter plate	Zentralabteilung für Technologie, Forschungszentrum Jülich, Germany
Glass bottom, Menzel-Gläser	Gerhard Menzel GmbH, Germany
UV Adhesive VERIFIX LV 740	Bohle AG, Germany
384 Wells glass microtiter plate	Mikroglas, Mainz, Germany

2.1.8 Labwares and instruments

Table 2-9: List of labwares and instruments

Labware/Instrument	Company
ÄKTApurifier	GE Healthcare, UK
AM TIRF system	Leica Microsystems, Germany
Cellulose Acetate Membrane Filter 0.2 µm	Sartorius AG, Germany
Lambda 25 UV/VIS spectrometer	Perkin Elmer, USA
LSM 710 microscope	Carl Zeiss AG, Germany
Plasma cleaner Zepto	Diener electronic, Ebhausen, Germany
Slide-A-Lyzer MINI Dialysis Devices, 10K MWCO	Thermo Fisher Scientific, USA
Superdex 200 10/300 GL column	GE Healthcare, UK
UVette cuvette	Eppendorf, Germany

2.1.9 Software

The analysis of protein sequences (molecular weight and extinction coefficient) was performed with the ProtParam tool (http://web.expasy.org/protparam/).

The images from confocal microscopy or total internal reflection fluorescence (TIRF) microscopy were analyzed by ImageJ or sFIDAta.

Table 2-10: List of softwares

Software	Company
Endnote X5	Thomson Reuters, Carlsbad, USA
GraphPad Prism 5.01	GraphPad Software, Inc., La Jolla, USA
ImageJ	National Institute of Health, USA (http://rsbweb.nih.gov/ij/)
LAS AF	Leica Microsystems, Germany
Microsoft Office 2010	Microsoft, Redmond, USA
Origin 8.5	OriginLab, Northampton, USA
sFIDAta	Institute of Complex System, Forschungszentrum Jülich, Germany
ZEN 2008	Carl Zeiss, Jena, Germany

2.2 Methods

2.2.1 Fluorescence labeling of antibodies

2.2.1.1 Fluorescence labeling with Alexa Fluor dyes

Antibody 6E10-Alexa Fluor 488 was purchased from Covance. For the purpose of multi-color imaging, a set of labeling kits including Alexa Fluor 488, 546 and 647 Monoclonal Antibody Labeling Kit as well as Alexa Fluor 633 Protein Labeling Kit were used to label the antibodies NAB228, IC16 (Table 2-3) respectively. The absorption and emission spectra of the four Alexa Fluor dyes are depicted in Figure 2-1.
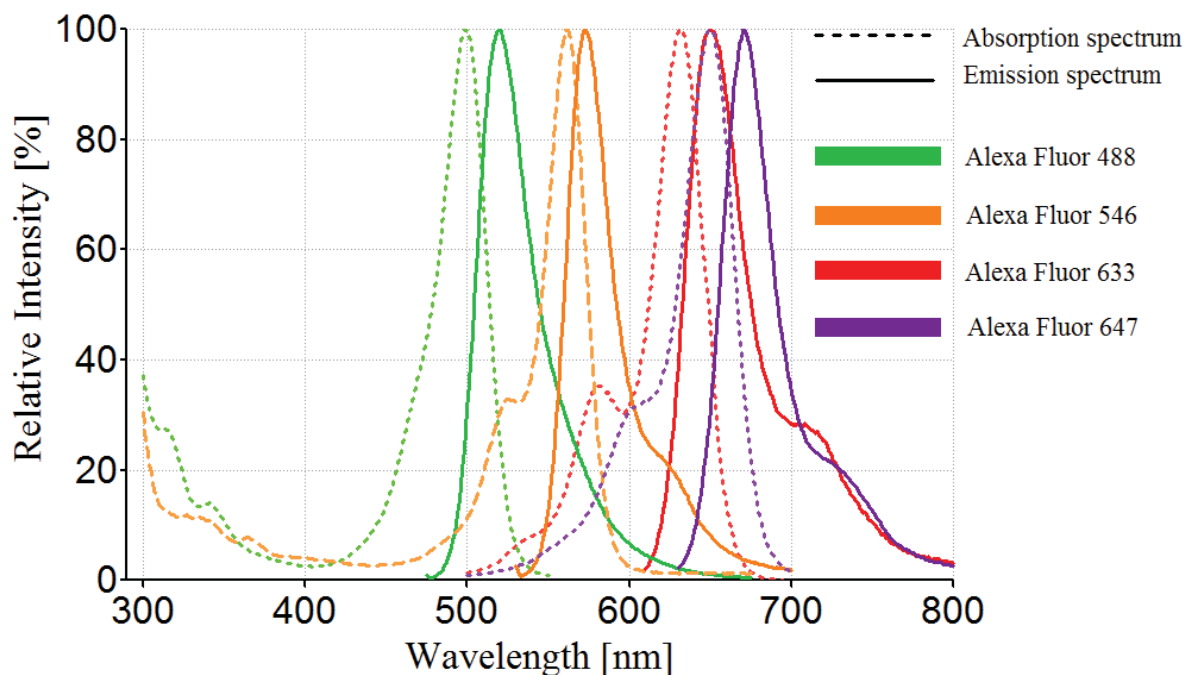
Figure 2-1: Absorption and emission spectra of Alexa Fluor dyes

The dotted lines depict fluorescence absorption spectra and the solid lines depict the fluorescence emission spectra. The lines in green color show the spectra of Alexa Fluor 488 dye; the lines in orange color show the spectra of Alexa Fluor 546 dye; the lines in red color show the spectra of Alexa Fluor 633 dye and the lines in purple color show the spectra of Alexa Fluor 647 dye (source: Spectral characteristics of Molecular Probes dyes, life technologies).

The antibodies were dialysed in PBS buffer with a dialysis device (Table 2-9) with a cut-off of 10,000 Da. The dialysis was performed in 1 L PBS buffer at 4 °C. The PBS buffer was changed per hour for three times. After the third time, the antibody solution was dialysed overnight. After the dialysis, 100 µg antibodies were then labeled using Antibody Labeling Kit following the instructions of the manufacturer.

After fluorescence labeling of the antibodies, the absorbance spectrum was measured in a plastic cuvette with a 1 cm path length (Table 2-9) on a spectrophotometer (Table 2-9) at 280 nm and 494 nm/554 nm/632 nm/650 nm. The protein concentration and the degree of labeling (mole number of dye per mole antibody) were calculated using Beer-Lambert law (Equation 2-1 and Equation 2-2).

Equation 2-1: Calculation of protein concentration

$$\text{Protein concentration } [M] = \frac{[A_{280} - (A_{494/554/632/650} \times f_c)] \times f_d}{203,000}$$

[M]	protein concentration is indicated in mol/L
A_{280}	the absorbance in a cuvette with a 1 cm pathlength at 280 nm
$A_{494/554/632/650}$	the absorbance in a cuvette with a 1 cm pathlength at 494 nm/554 nm/632 nm/650 nm
203,000	the molar extinction coefficient (ε) in $cm^{-1}M^{-1}$ of a typical IgG at 280 nm
f_d	dilution factor
f_c	correction factor for the fluorophore's contribution to the absorbance at 280 nm
	f_c = 0.11 for Alexa Fluor 488
	f_c = 0.12 for Alexa Fluor 546
	f_c = 0.55 for Alexa Fluor 633
	f_c = 0.03 for Alexa Fluor 647

Equation 2-2: Calculation of the degree of labeling

$$\text{Moles dye per mole protein} = \frac{A_{494/554/632/650} \times f_d}{\varepsilon \times \text{Protein concentration } [M]}$$

ε the molar extinction coefficient in cm^{-1}M^{-1} of Alexa Fluor dye

ε = 71,000 for Alexa Fluor 488 at 494 nm

ε = 104,000 for Alexa Fluor 546 at 554 nm

ε = 100,000 for Alexa Fluor 633 at 632 nm

ε = 239,000 for Alexa Fluor 647 at 650 nm

2.2.1.2 Fluorescence labeling with ATTO dyes

Antibodies 6E10, IC16 (Table 2-3) were labeled using ATTO 488 and 647N (NHS-Ester) (Table 2-7). The absorption and emission spectra of ATTO dyes are depicted in Figure 2-2.
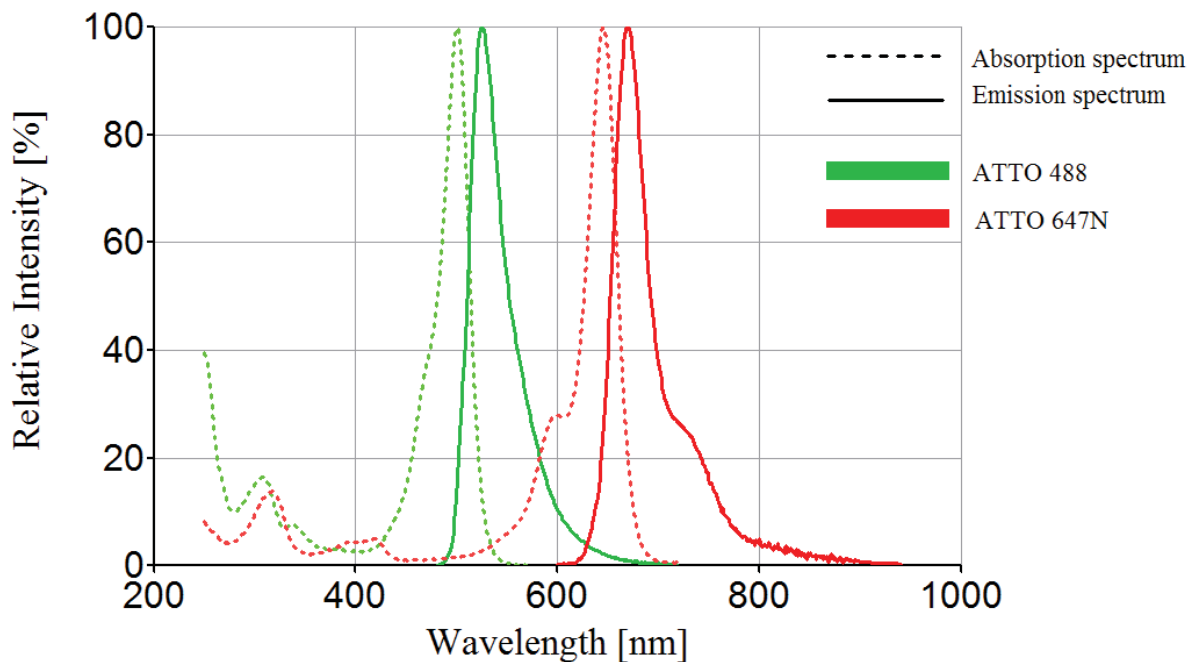
Figure 2-2: Absorption and emission spectra of ATTO dyes

The dotted lines depict fluorescence absorption spectra and the solid lines depict the fluorescence emission spectra. The lines in green color show the spectra of ATTO 488 dye and the lines in red color show the spectra of ATTO 647N dye (source: ATTO-TEC GmbH).

The antibodies were dialysed in PBS buffer with a dialysis device (Table 2-9) with a cut-off of 10,000 Da. The dialysis was performed in 1 L PBS buffer at 4 °C. The PBS buffer was changed per hour for three times. After the third time, the antibody solution was dialysed overnight. After the dialysis, 100 µg antibodies were then labeled using ATTO dye following the instructions of the manufacturer.

After fluorescence labeling of the antibodies, the absorbance spectrum was measured in a plastic cuvette with a 1 cm path length (Table 2-9) on a spectrophotometer (Table 2-9) at 280 nm and 523 nm/669 nm. The protein

concentration and the degree of labeling (mole number of dye per mole antibody) were calculated using Beer-Lambert law (Equation 2-3 and Equation 2-4).

Equation 2-3: Calculation of protein concentration

$$\text{Protein concentration} \left[M\right] = \frac{\left[A_{280} - \left(A_{523/669} \times f_c\right)\right] \times f_d}{203{,}000}$$

[M]	protein concentration is indicated in mol/L
A_{280}	the absorbance in a cuvette with a 1 cm pathlength at 280 nm
$A_{523/669}$	the absorbance in a cuvette with a 1 cm pathlength at 523 nm/669 nm
203,000	the molar extinction coefficient (ε) in $cm^{-1}M^{-1}$ of a typical IgG at 280 nm
f_d	dilution factor
f_c	correction factor for the fluorophore's contribution to the absorbance at 280 nm
	f_c = 0.10 for ATTO 488
	f_c = 0.05 for ATTO 647N

Equation 2-4: Calculation of the degree of labeling

$$\text{Moles dye per mole protein} = \frac{A_{523/669} \times f_d}{\varepsilon \times \text{Protein concentration} \left[M\right]}$$

ε	the molar extinction coefficient in $cm^{-1}M^{-1}$ of Alexa Fluor dye
	ε = 90,000 for ATTO 488 at 523 nm
	ε = 150,000 for ATTO 647N at 669 nm

2.2.2 Preparation of 16- and 32-branched multiple antigenic peptide

The synthetic multiple antigenic peptide (MAP) molecules consist of multiple units of the amino acids 1-11 of the human amyloid-β protein. The epitopes are linked to a branching lysine core to produce 4- or 8-branched multiple antigenic peptide (4MAP or 8MAP). However, it is challenging to (chemically) synthesize MAP molecules with more epitopes such as 16-mer or even 32-mer. Therefore, 16MAP and 32MAP were constructed based on the interaction of the biotin tag on 4MAP or 8MAP with the streptavidin (Table 2-1). And one tetrameric streptavidin molecule can bind up to four 4MAP or 8MAP molecules.

2.2.2.1 Preparation of 16MAP

4MAP peptides were dissolved in 100 µl phosphate buffered saline (PBS) to a concentration of 0.157 mM, streptavidin was dissolved in 50 µl PBS to a concentration of 0.067 mM. 100 µl 4MAP solution and 50 µl streptavidin solution were then mixed and incubated for 3 h at room temperature.

2.2.2.2 Preparation of 32MAP

8MAP peptides were dissolved in 100 µl phosphate buffered saline (PBS) to a concentration of 0.171 mM, streptavidin was dissolved in 50 µl PBS to a concentration of 0.067 mM. 100 µl 8MAP solution and 50 µl streptavidin solution were then mixed and incubated for 3 h at room temperature.

2.2.2.3 Purification of 16MAP and 32MAP using size exclusion chromatography

Size exclusion chromatography (SEC) is a chromatographic method to separate molecules based on their different sizes. SEC was used to purify 16MAP and 32MAP.

All solutions used for SEC were filtered by 0.2 µm membrane filter (Table 2-9) and degased. Äkta system (Table 2-9) and a Superdex 200 10/300 GL column (Table 2-9) were used for SEC. After the sample run the column was cleaned with 0.5 M NaOH, 0.5 M acetic acid, and water respectively and then stored in 20% ethanol.

The reaction mix of 4MAP and streptavidin as well as 8MAP and streptavidin described above (see 2.2.2) was centrifuged for 5 min at 16,100 x g. 140 µl of supernatant were injected to the SEC column. The samples were eluted at room temperature, at a flow rate of 0.5 ml/min with PBS. The elution absorption was monitored at 214 nm and 280 nm.

The absorbance spectra of eluted fractions of SEC were measured in a plastic cuvette with a 1 cm path length on a spectrophotometer at 280 nm. The peptide concentration was calculated using Beer-Lambert law (Equation 2-1).

2.2.3 Preparation of synthetic Aβ aggregates

The preparation of Aβ aggregates was performed in low binding tubes. Lyophilized Aβ peptides were dissolved in 1,1,1,3,3,3-hexafluoro-2-propanol (HFIP) to a concentration of 400 µM and incubated overnight at room temperature to dissolve pre-existing aggregation seeds. Afterwards, the solution was aliquoted and let the HFIP evaporate. The aliquots were stored at -80 ℃. The Aβ film was re-dissolved in 5.3 mM NaOH for 10 min, then the Aβ solution was diluted in PBS and 4.7 mM HCl to a final concentration of 40 µM (protocol according to Schlenzig et al., 2009). The preparation was incubated for at least 12 h at 37 ℃. The solutions were further diluted in PBS to the desired concentrations.

2.2.4 sFIDA protocol

96-well glass microtiter plate or 384-well glass microtiter plate was used for the sFIDA protocol. The plate was first cleaned with ethanol and double-distilled water (ddH$_2$O), respectively. The wells were filled with 45 µl 5 M NaOH and incubated for 3 h. After the incubation the wells were washed five times with ddH$_2$O and dried. The plate was then treated in the plasma cleaner (Table 2-9). Immediately 5 M ethanolamine in DMSO was added to the wells and incubated overnight at room temperature (Ebner et al., 2007).

The wells were washed five times with ddH$_2$O. Carboxymethyl dextran sodium salt (CMD) was dissolved in PBS (10 mg/ml) and filtrated with 0.2 µm filter, then CMD solution was centrifuged at 20,000 g for 10 min. The CMD was then incubated with 200 mM EDC and 50 mM NHS for 10 min. 45 µl of the CMD/EDC/NHS solution were added to each well and incubated for 1 h. After washing the wells with PBS for five times, 15 µl EDC/NHS (200/50 mM in PBS) were added to each well and incubated for 10 min. After washing three times with ddH$_2$O, 15 µl capture antibody NAB228 (0.01 µg/ µl in PBS) were added to each well and incubated for 30 min at room temperature.

The antibody solution was then removed and 45 µl ethanolamine hydrochloride (0.1 M in PBS, pH 7.4) were added to the wells and incubated for 10 min. Following were

three times washing of TBS and three times washing of TBST respectively. Samples were added to the wells with 15 µl per well and incubated for 1 h at room temperature.

The wells were washed with TBS two times. The two fluorescence labeled detection antibodies (see 2.2.1) were diluted in TBS to a concentration of 0.00125 µg/µl for each in a mixture and centrifuged at 20,000 g for 10 min. Then 15 µl of the detection antibodies were added to each well and incubated for 60 min at room temperature. The wells were then washed one time with TBST, one time with TBS and one time with ddH$_2$O respectively. Fluorescence signals were then measured by confocal or total internal reflection fluorescence (TIRF) microscopy.

2.2.5 Confocal microscopy

Confocal microscopy was performed using the confocal laser scanning microscope (LSM) LSM710 equipped with a diode laser (excitation wavelength 405 nm), an argon ion laser (excitation wavelengths 458, 488 and 514 nm), a DPSS laser (excitation wavelength 561 nm) and a helium-neon laser (excitation wavelengths 594 and 633 nm). Specimens are imaged with a 40× objective (Zeiss, 1.3 NA oil immersion lens) of an inverted fluorescence microscope (Zeiss Axio Observer.Z1 SP). The fluorescence light emitted by the scanned specimen is collected by a photomultiplier tube (PMT). The Zen 2008 software (Carl Zeiss, Jena, Germany) was used to control the system.

2.2.6 Total internal reflection fluorescence (TIRF) microscopy

Total internal reflection fluorescence (TIRF) microscopy was performed on a Leica AM TIRF system (Table 2-9). The system includes a MC laser box which has excitation wavelengths 405, 488, 561 and 635 nm. The samples were measured with an inverted microscope (Leica DMI6000 B) equipped with a 100× objective (Leica, 1.47 NA oil immersion lens). The images were acquired by an electron-multiplying charge-coupled device (EM-CCD) camera (Hamamatsu, C9100). The Leica LAS AF software (Table 2-10) was used to control the system.

2.2.7 Image analysis

The open source software ImageJ was used to analyze the image data. Further introduction of sFIDAta, provided an integrated solution for the analysis of the images.

The detector (PMT or EM-CCD) of the microscope received fluorescence signals from the two detection probes through distinct fluorescence channels. A histogram analysis showed the pixel count above each intensity threshold covering the whole range of the grayscale of one fluorescence channel. Based on the histogram analysis, certain intensity cut-off value was set to distinguish different samples.

The fluorescence signals were detected in two distinct fluorescence channels. And colocalization events occurred when signals from the two fluorescence channels overlapped at the same pixel location. The term "sFIDA readout" is defined as the quantitative value of the pixel count of all colocalization events above a certain intensity cut-off in one single scanning area or the averaged value of multiple scanning areas.

Statistical analyses were performed by the software GraphPad Prism 5.01 (see 2.1.9). The unpaired student's t-test (95% confidence interval) was used for the comparison between two sample groups. When P value is less than 0.05, the means are considered significantly different.

2.2.8 Capture antibody competition

A series of mixtures of two components (Table 2-11), the fluorescence labeled antibody 6E10-Alexa Fluor 488 (Table 2-3) and the unlabeled monoclonal antibody NAB228 (Table 2-3), were applied to the activated glass surface which was treated according to sFIDA protocol (see 2.2.4). The protocol for this experiment included the standard steps of the sFIDA protocol till the step of capture antibody incubation, followed by an additional step of 1% sodium dodecyl sulfate (SDS) washing to remove non-covalently bound antibodies. The plate was then measured by TIRF microscopy (see 2.2.6).

Table 2-11: Mixture of the antibodies

Sample no.	1	2	3	4	5	6	7	8	9
6E10-Alexa Fluor 488 (μg/μl)	0.001	0.001	0.001	0.001	0.001	0.001	0.001	0.001	0.001
NAB228 (μg/μl)	0	0.005	0.010	0.020	0.030	0.040	0.060	0.080	0.100

3 Results

A reliable preclinical diagnosis is an indispensable prerequisite in the fight against Alzheimer's disease (AD). In this context surface-based-fluorescence intensity distribution analysis (sFIDA) has emerged as a valuable method for the detection of amyloid-β (Aβ) oligomers in body fluid samples. Initially sFIDA was established on fluorescence correlation spectroscopy (FCS) and later was adapted to confocal laser scanning microscopy (LSM).

In this work, sFIDA assay was established on total internal reflection fluorescence (TIRF) microscopy. In comparison with FCS and LSM, TIRF microscopy has provided high resolution images plus fast and automated multi-well imaging.

Previous work suggested Aβ as an important biomarker of AD. In an earlier study sFIDA was able to distinguish the different types of human CSF (control, MCI and AD). A main object of this work is to validate the performance of sFIDA on various sample pools. Human CSF samples purchased from Biochemed and human CSF samples provided by the collaboration partner Prof. Piotr Lewczuk from Universitätsklinikum Erlangen have been measured and analyzed.

The performance of sFIDA is dependent on the quality of the capture antibodies bound to the surface, as the capture antibodies are responsible for immobilizing the Aβ oligomers. One of the concerns was whether the capture antibodies distributed homogeneously on the surface. For this end fluorescence labeled capture antibodies were applied to the surface. The fluorescence signals were then detected and they visualized the distribution of the capture antibodies. Another concern was the amount of capture antibody which was covalently immobilized on the surface. Capture antibody competition experiment helped optimize the concentration of capture antibody used in the sFIDA protocol.

A reference system is needed for sFIDA so that different measurements could be compared quantitatively. Multiple antigenic peptide (MAP) molecules with 16 or 32 units of epitopes have been developed and constructed in this work. And the MAP molecule was tested for its potential as a reference standard to calibrate sFIDA assay.

3.1 Adaption of sFIDA to TIRF microscopy

In previous studies, sFIDA was established on confocal microscopy (Wang-Dietrich et al., 2013). The size, shape and composition of the Aβ aggregates could be analyzed. However, there are disadvantages. First, it takes the confocal microscope LSM710 approximately 20 seconds to scan one single image (two fluorescence channels, 212 µm × 212 µm in size, 1024 pixels × 1024 pixels). Second, the multiple-well scanning function is not fully automated with the setup of LSM710. To overcome those advantages, TIRF microscopy was introduced to sFIDA assay.

There are several advantages of the TIRF microscopy. Firstly, it only takes approximately 2 seconds for taking one single image (two fluorescence channels, 114 µm × 114 µm, 1000 pixels × 1000 pixels). This has greatly increased the throughput of the assay. Secondly, the motor-driven platform and the autofocus function operated by the Leica software enable fully automated imaging for multiple wells. This greatly saves time for the operator. As one of the super-resolution light microscopy methods, the excitation mechanism of TIRF allows fluorophores to be exclusively excited in a range of approximately some hundred nanometers above the glass-media interface. In this way the signal-to-noise ratio is promoted.

Synthetic Aβ aggregates were prepared as described (see 2.2.3). 5 µM Aβ aggregates were immobilized onto the glass surface according to the sFIDA protocol (see 2.2.4). PBS was used as the buffer control. The fluorescence labeled antibodies 6E10-Alexa Fluor 488 and IC16-Alexa Fluor 647 were used for the detection. Measurements were performed by both TIRF microscopy and confocal LSM. The images of Aβ aggregates from TIRF microscopy are shown in Figure 3-1. The images of Aβ aggregates from confocal LSM are shown in Figure 3-2. Colocalized particles are observed in the images from both TIRF microscopy and confocal LSM. The images of PBS control from both TIRF microscopy and confocal LSM are shown in Figure 3-3 and no significant fluorescence signals were detected. This suggested that the Aβ aggregates were recognized by both detection antibodies. Therefore the sFIDA assay was successfully established on TIRF microscopy, and it was ready to measure real biological samples.
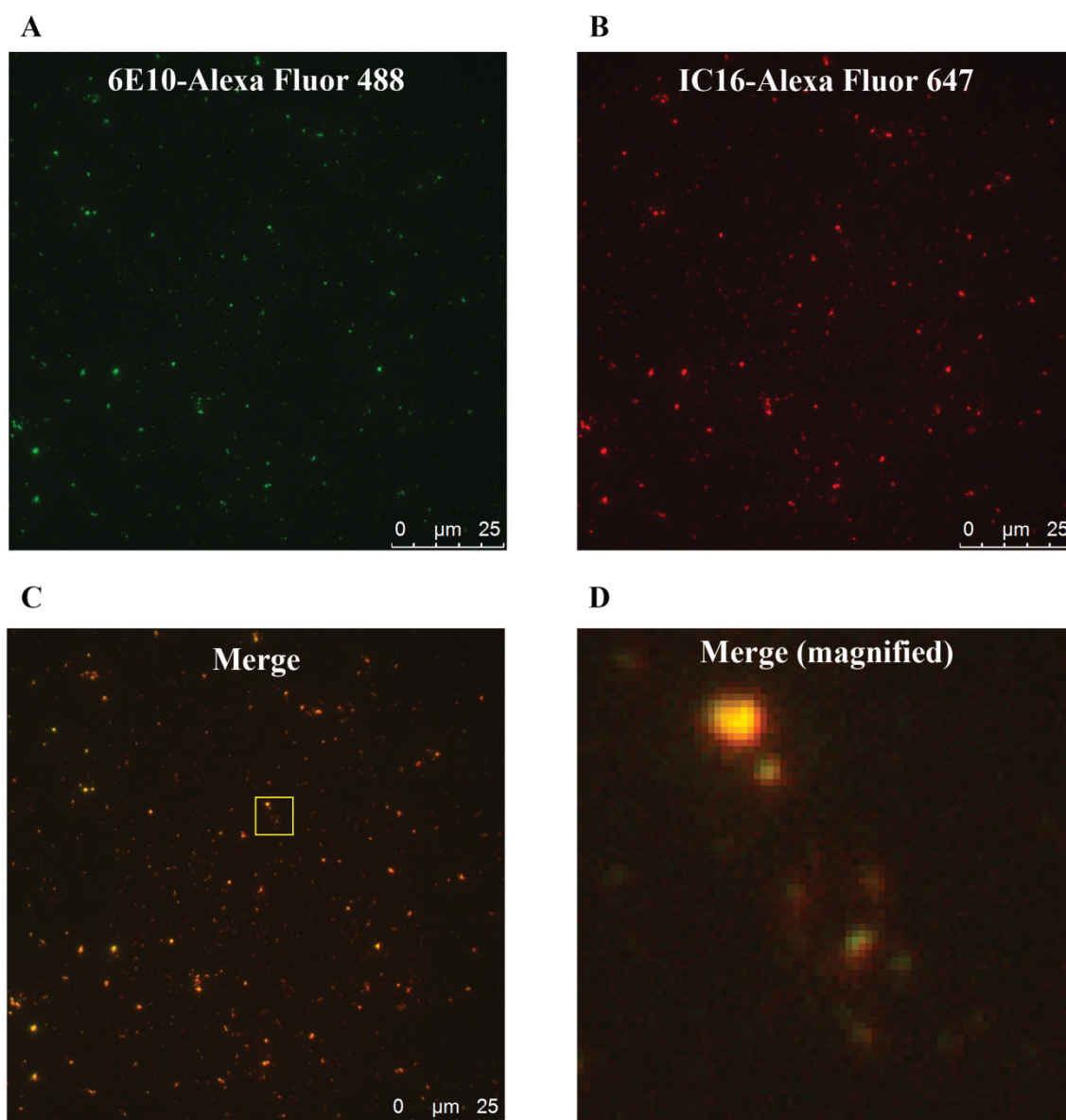
Figure 3-1: TIRF Images of Aβ aggregates

5 µM Aβ aggregates were immobilized onto the glass surface. The images were taken by TIRF microscopy. (A) Aβ aggregates detected by antibody 6E10-Alexa Fluor 488 in the green channel. (B) Aβ Aggregates detected by antibody IC16-Alexa Fluor 647 in the red channel. (C) The merge of green and red channel. (D) The yellow line marked rectangle area in (C) was magnified. Scale bar is 25 µm.

A

6E10-Alexa Fluor 488

50 μm

B

IC16-Alexa Fluor 647

50 μm

C

Merge

50 μm

D

Merge (magnified)
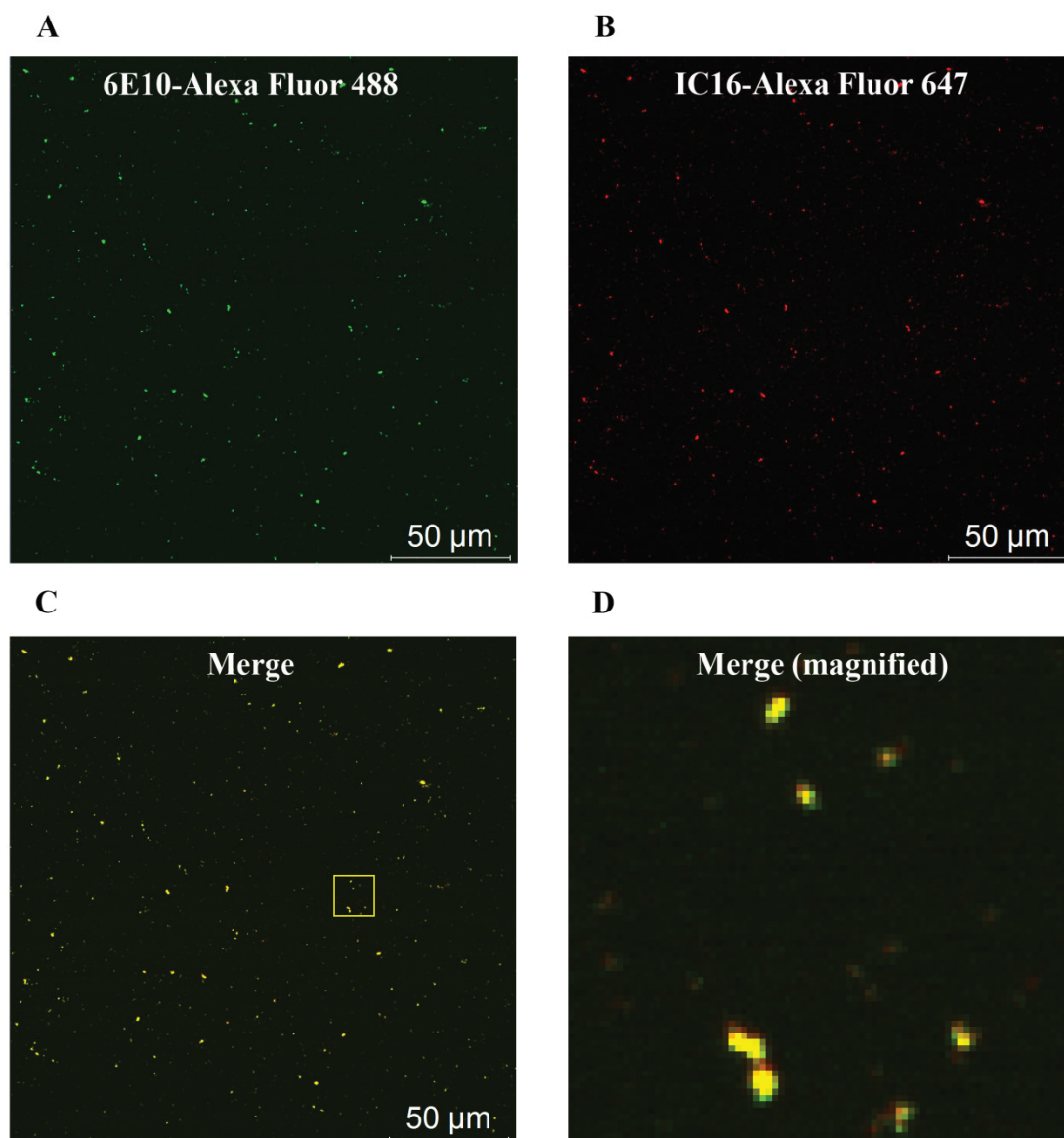
Figure 3-2: LSM Images of Aβ aggregates

5 μM Aβ aggregates were immobilized onto the glass surface. The images were taken by confocal LSM. (A) Aβ aggregates detected by antibody 6E10-Alexa Fluor 488 in the green channel. (B) Aβ aggregates detected by antibody IC16-Alexa Fluor 647 in the red channel. (C) The merge of green and red channel. (D) The yellow line marked rectangle area in (C) was magnified. Scale bar is 50 μm.
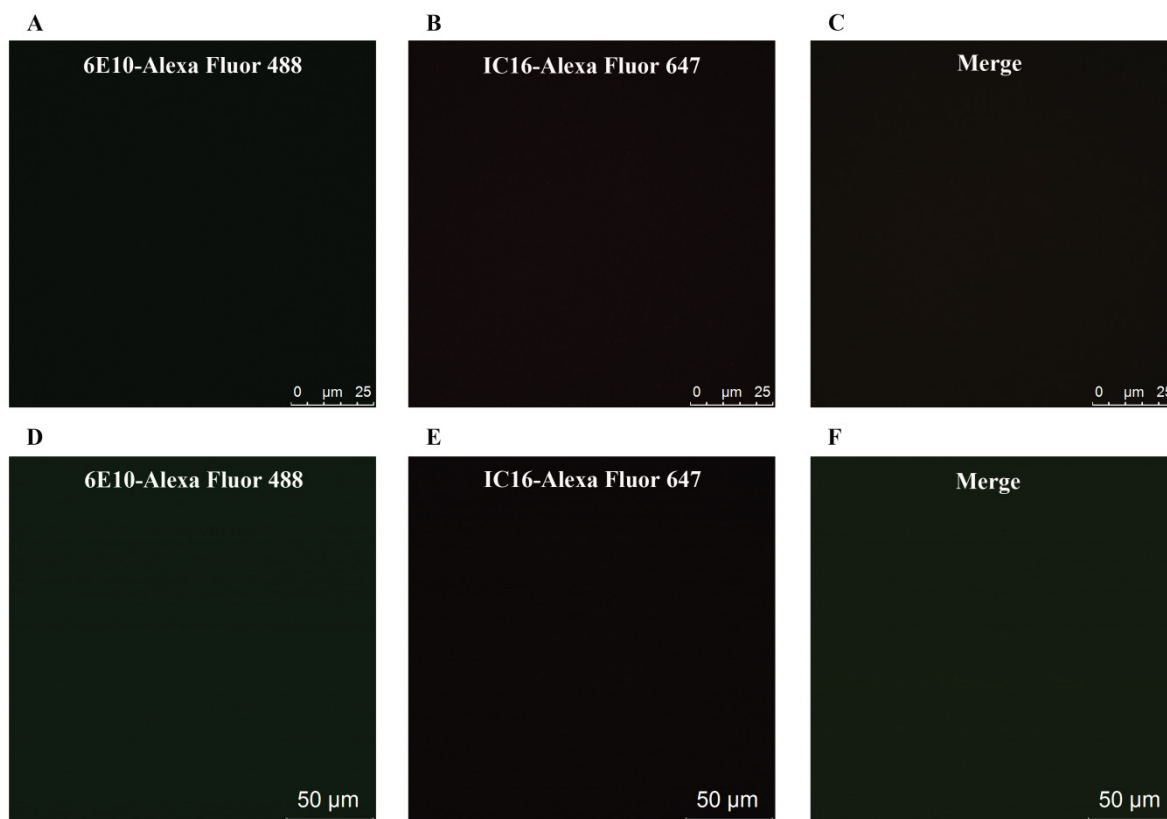
Figure 3-3: TIRF and LSM Images of PBS control

PBS was applied as the buffer control. The images were taken by TIRF microscopy (A, B, C) and confocal LSM (D, E, F). (A, D) Green channel corresponds to the detection by antibody 6E10-Alexa Fluor 488. (B, E) Red channel corresponds to the detection by antibody IC16-Alexa Fluor 647. (C, F) The merge of green and red channel. Scale bar is 25 μm (A, B, C) or 50 μm (D, E, F).

3.2 sFIDA measurement of human CSF samples

Human CSF samples from different sources were measured and analyzed by sFIDA to evaluate the ability of sFIDA on distinguishing those samples. CSF samples purchased from Biochemed were derived from control and AD positive individuals (Table 2-5). And the CSF samples from the collaboration partner Prof. Piotr Lewczuk from Universitätsklinikum Erlangen included AD, MCI and control types (Table 2-6).

3.2.1 Commercial human CSF samples (Biochemed)

The donors of the CSF samples from Biochemed comprised of five control and five AD positive individuals (Table 2-5). The sFIDA protocol (see 2.2.4) was performed on a ZAT microtiter plate. The antibodies 6E10-ATTO 488 and IC16-ATTO 647 were used for detection. The fluorescence signals were then measured by TIRF microscopy. The imaging of each sample well includes 25 single images covering an area in the form of a 5×5 matrix. The fluorescence signals from the two detection antibodies through separate fluorescence channels were received and recorded by the detector of the microscope. Colocalization is defined as the signals from the two fluorescence channels overlapped at the pixel of the same location. The term "sFIDA readout" is defined as the quantitative value of the pixel count of all colocalized events above a certain intensity cut-off. The sFIDA readout refers to the value of one single scanning area or the averaged value of multiple scanning areas.

Figure 3-4A shows the box-and-whisker plot comprising of sFIDA readout data of each individual of the five control and five AD positive samples. Each data value represents the sFIDA readout of one scanning area i.e. one single image. The control samples show lower fluorescence signals than those of the AD samples except for Control 31-6.

Figure 3-4B shows the sFIDA readout data of the five control samples as a group and the five AD samples as a group. Each data point represents the averaged sFIDA readout value of one individual sample. Despite the high signal of Control 31-6, there is a significant difference between the control and AD groups (p = 0.0151, student's t-test). And via visual observation, the sFIDA values could be related to the fluorescence signals demonstrated by some representative images of samples Control 21-8 and Control 31-6 (Figure 3-5), AD 0367 and AD 378 (Figure 3-6).
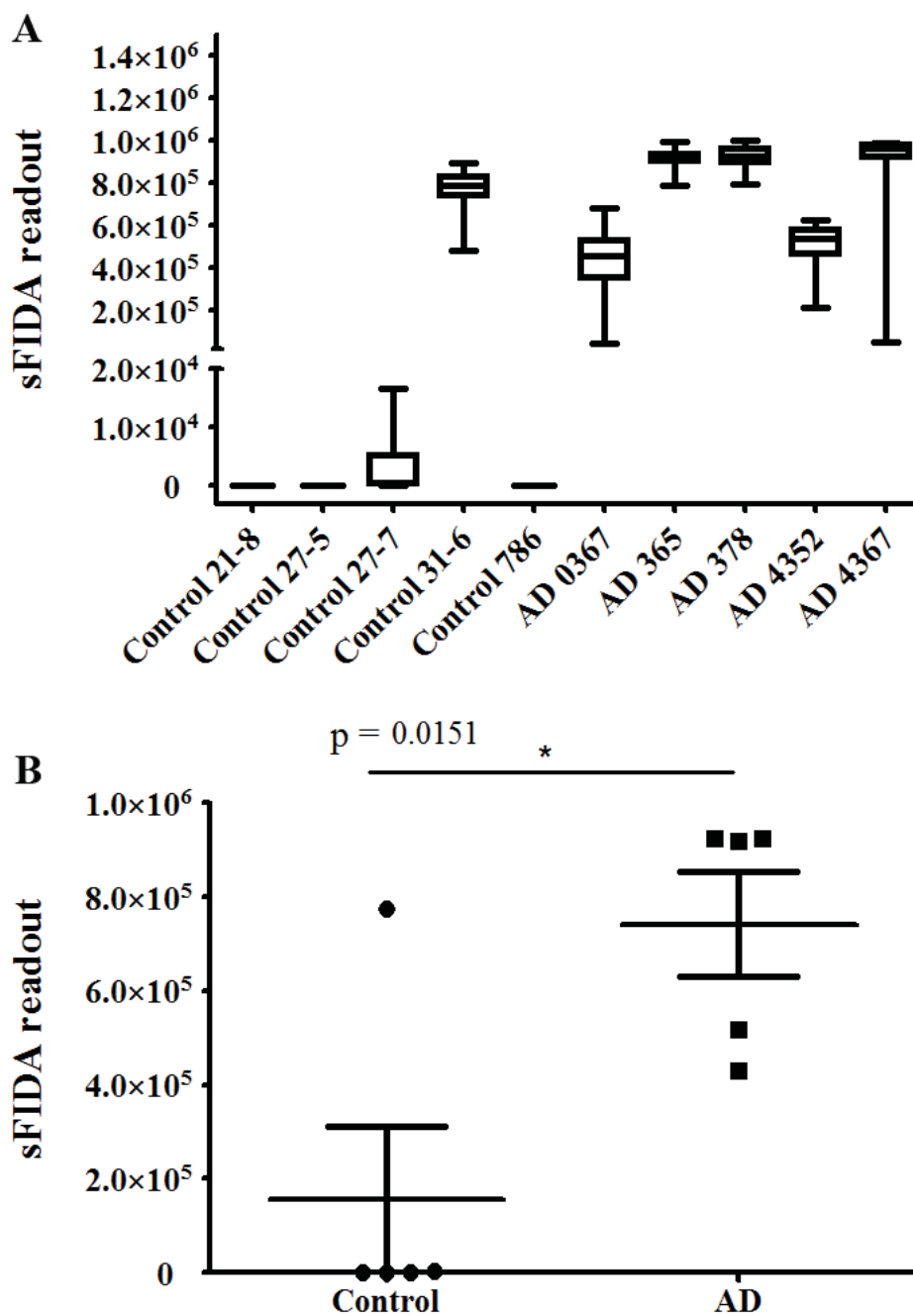
Figure 3-4: sFIDA results of the human CSF samples (Biochemed)

Five control and five AD samples were subjected to sFIDA analysis. (A) sFIDA readout data of all individual samples.The sFIDA readout values of each single image were used to show the distribution of the values of the multiple images of the same sample. Each data value of the box-and-whisker plot represents one scanning area i.e. one single image. (B) sFIDA readout data of the five control samples as a group and the five AD samples as a group. The sFIDA readout values of the multiple images of the same sample were averaged and the mean sFIDA readout values were plotted. Each data point represents one individual sample. The student's t-test (95% confidence interval) was used for the statistical analysis.

34
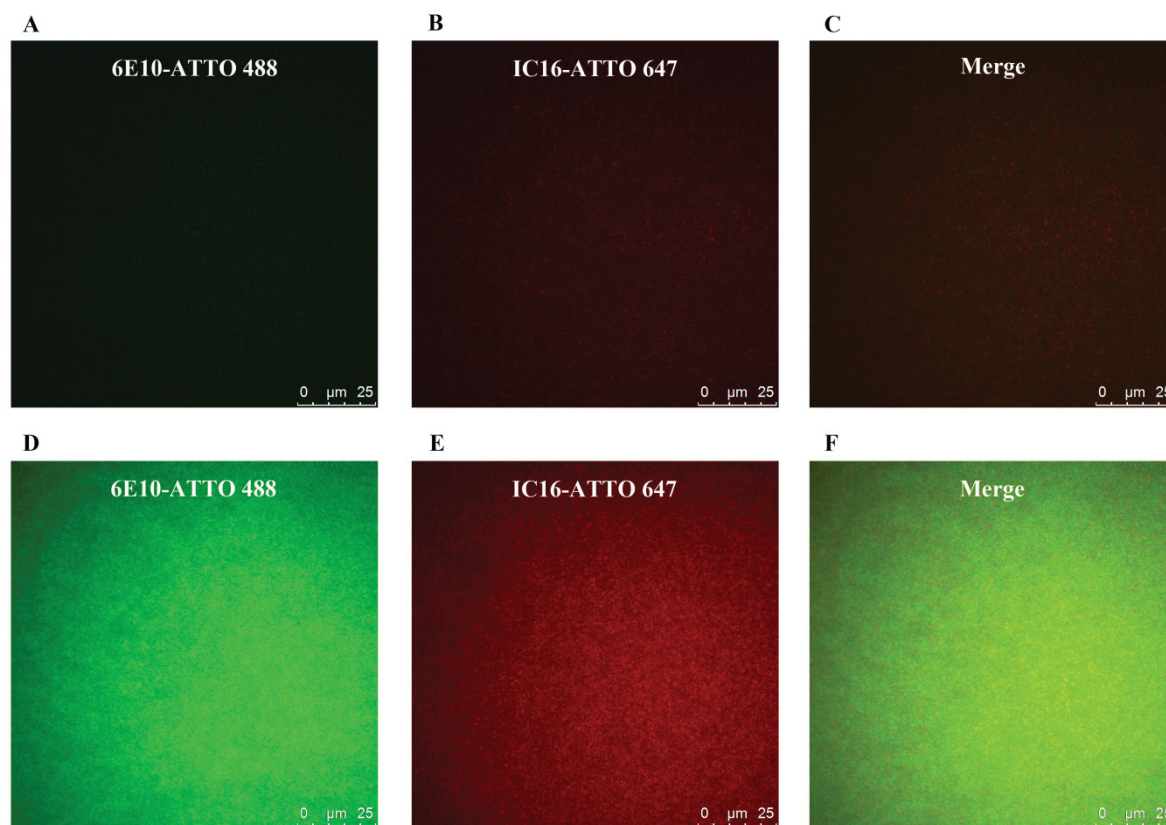
Figure 3-5: TIRF Images of human CSF samples Control 21-8 and Control 31-6

The images were taken by TIRF microscopy. (A, B, C) The images of one single scanning area of Control 21-8. (C, D, E) The images of one single scanning area of Control 31-6. (A, D) Green channel corresponds to the detection by antibody 6E10-ATTO 488. (B, E) Red channel corresponds to the detection by antibody IC16-ATTO 647. (C, F) The merge of green and red channel. Scale bar is 25 µm.
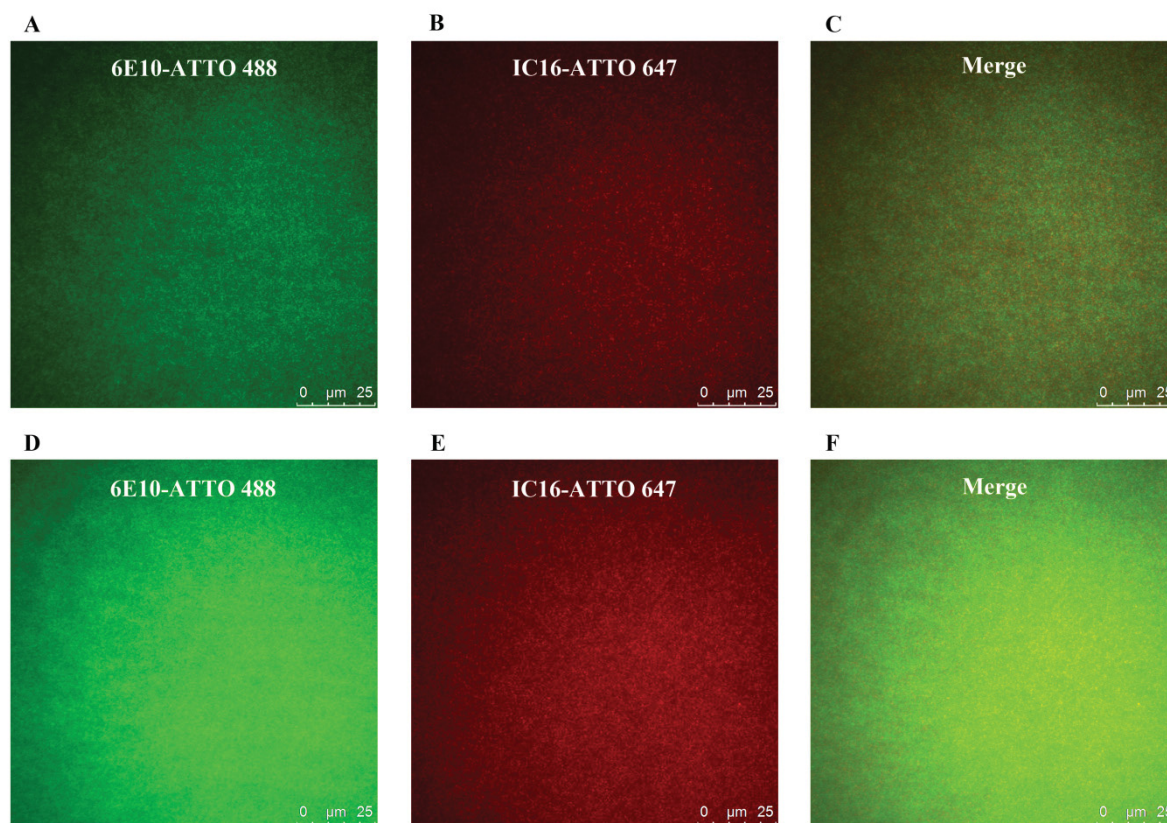
Figure 3-6: TIRF Images of human CSF samples AD 0367 and AD 378

The images were taken by TIRF microscopy. (A, B, C) The images of one single scanning area of AD 0367. (C, D, E) The images of one single scanning area of AD 378. (A, D) Green channel corresponds to the detection by antibody 6E10-ATTO 488. (B, E) Red channel corresponds to the detection by antibody IC16-ATTO 647. (C, F) The merge of green and red channel. Scale bar is 25 µm.

3.2.2 Human CSF from Universitätsklinikum Erlangen

19 CSF samples (10 control, 6 MCI and 3 AD subjects, Table 2-6) from Prof. Piotr Lewczuk of Universitätsklinikum Erlangen were measured in two independent experiments. 8 of those 19 samples were measured in experiment 1, while all 19 samples were measured in experiment 2.

The sFIDA protocol (see 2.2.4) was performed on a ZAT microtiter plate. The antibodies 6E10-ATTO 488 and IC16-ATTO 647 were used for detection. The fluorescence signals were then measured by TIRF microscopy.

8 samples (4 control, 2 MCI and 2 AD subjects) were measured in experiment 1. In Figure 3-7 the sFIDA readout values from multiple images of the same sample were averaged and the mean sFIDA readout values were plotted. The control, MCI and AD groups could not be significantly distinguished. The signals from the control samples showed a rather heterogeneous pattern. The representative images of samples Control 042 and Control 136 (Figure 3-8), MCI 160 and AD 047 (Figure 3-9) were shown, and the fluorescence signals of those images were in accordance with the corresponding sFIDA readout values.

Figure 3-7: Analysis of 8 CSF samples in experiment 1

sFIDA readout data of 4 control, 2 MCI and 2 AD samples. The sFIDA readout values from multiple images of the same sample were averaged and the mean sFIDA readout values were plotted. Each data point represents one individual sample. The student's t-test (95% confidence interval) was used for the statistical analysis. "ns" means no significant difference.

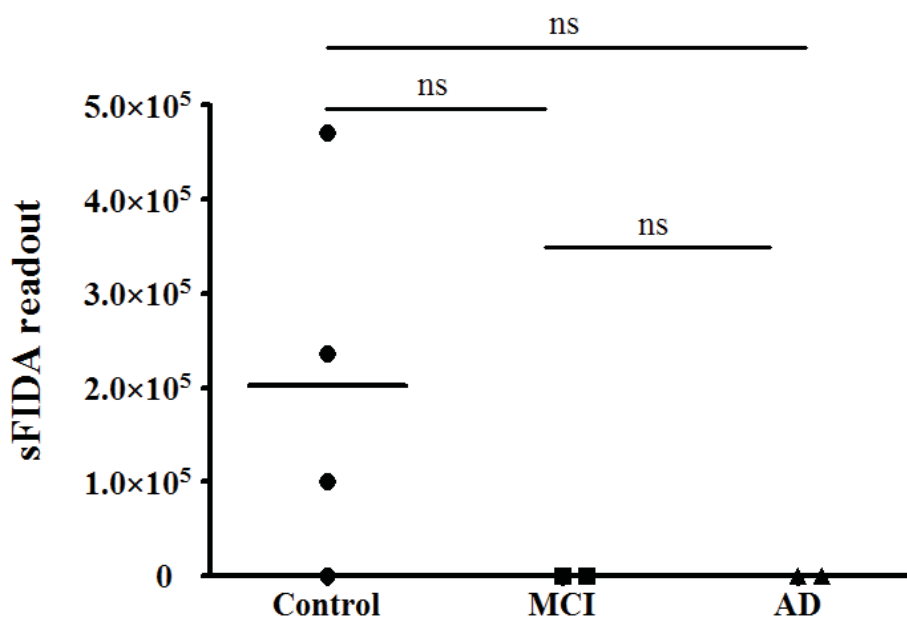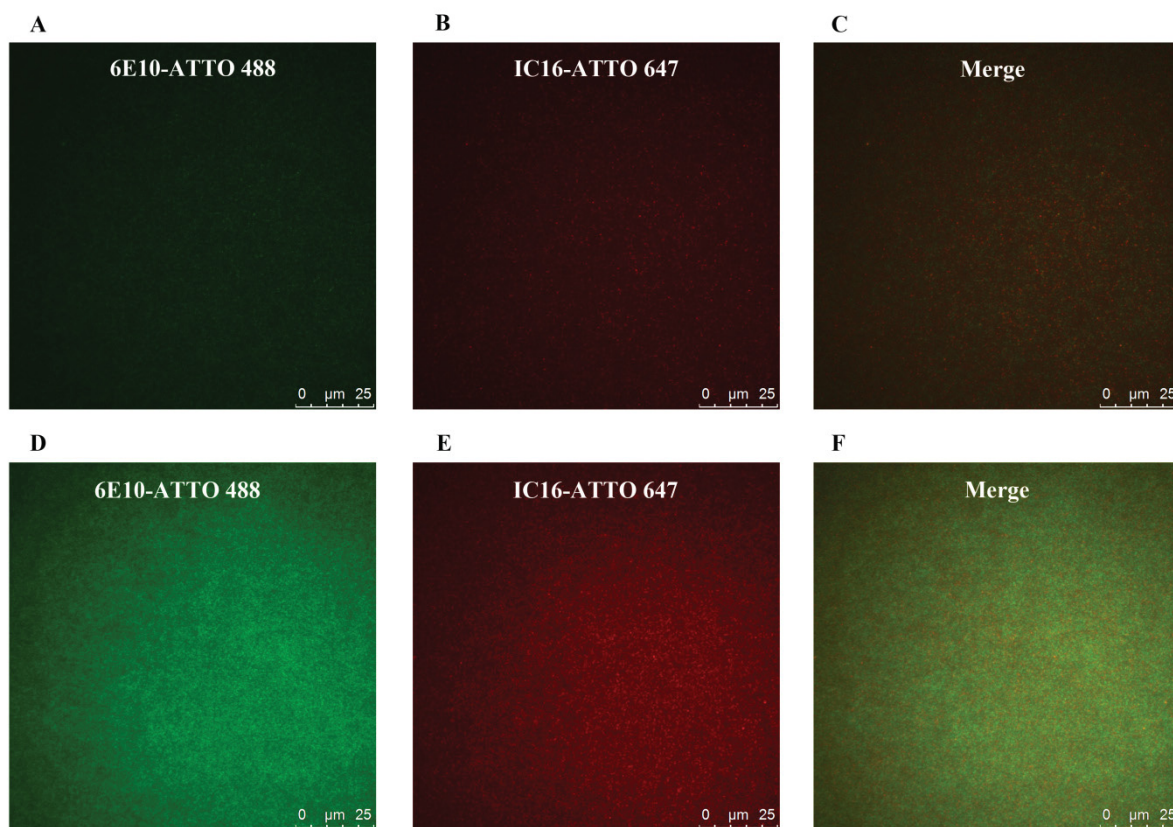**Figure 3-8: TIRF Images of human CSF samples Control 042 and Control 136**

The images were taken by TIRF microscopy. (A, B, C) The images of one single scanning area of Control 042. (C, D, E) The images of one single scanning area of Control 136. (A, D) Green channel corresponds to the detection by antibody 6E10-ATTO 488. (B, E) Red channel corresponds to the detection by antibody IC16-ATTO 647. (C, F) The merge of green and red channel. Scale bar is 25 µm.

Figure 3-9: TIRF Images of human CSF samples MCI 160 and AD 047

The images were taken by TIRF microscopy. (A, B, C) The images of one single scanning area of MCI 160. (C, D, E) The images of one single scanning area of AD 047. (A, D) Green channel corresponds to the detection by antibody 6E10-ATTO 488. (B, E) Red channel corresponds to the detection by antibody IC16-ATTO 647. (C, F) The merge of green and red channel. Scale bar is 25 µm.

19 samples (10 control, 6 MCI and 3 AD subjects) were measured in experiment 2. In Figure 3-10 the sFIDA readout values from multiple images of the same sample were averaged and the mean sFIDA readout values were plotted. MCI and AD samples showed lower signals in comparison to the control samples. And control samples showed heterogeneous signals. The control group and MCI group could be significantly distinguished (p = 0.0162, student's t-test), while none of the other group pairs could be significantly distinguished.
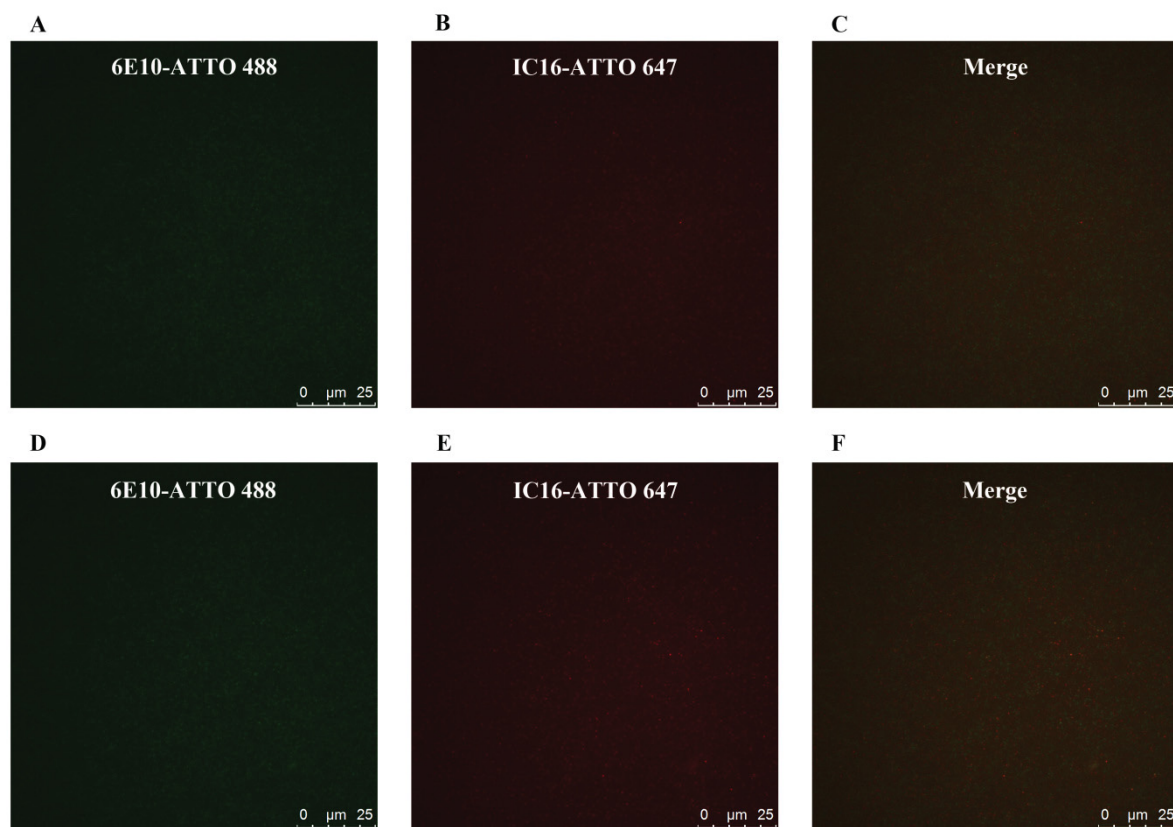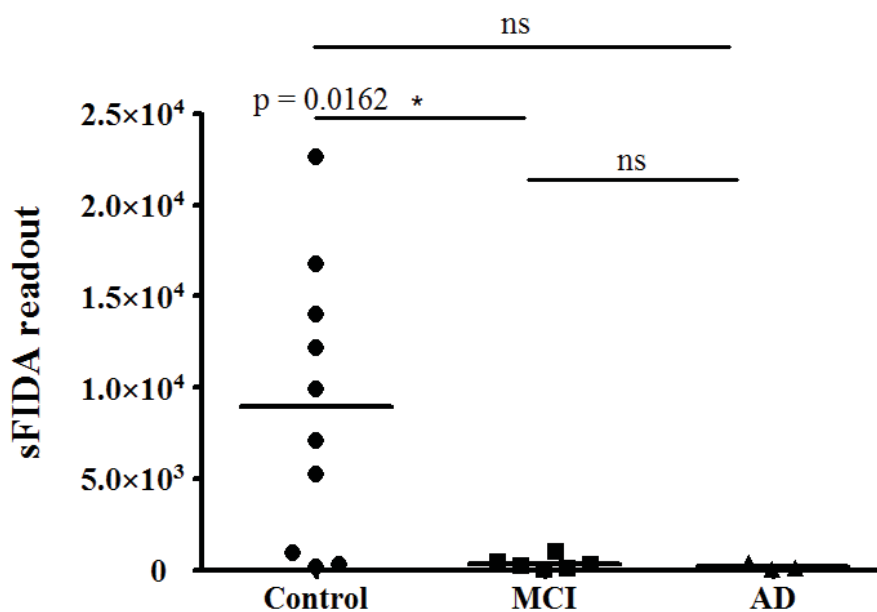

Figure 3-10: Analysis of 19 CSF samples in experiment 2

sFIDA readout data of 10 control, 6 MCI and 3 AD samples. The sFIDA readout values from multiple images of the same sample were averaged and the mean sFIDA readout values were plotted. Each data point represents one individual sample. The student's t-test (95% confidence interval) was used for the statistical analysis. "ns" means no significant difference.

Correlation analysis was performed on the sFIDA readout values of the same 8 samples measured in both experiment 1 and experiment 2 (Figure 3-11). There is a significant correlation between the sFIDA readout values from the two experiments (two-tailed $p = 0.0218$, Spearman $r = 0.8095$). This suggests the two experiments were reproducible.
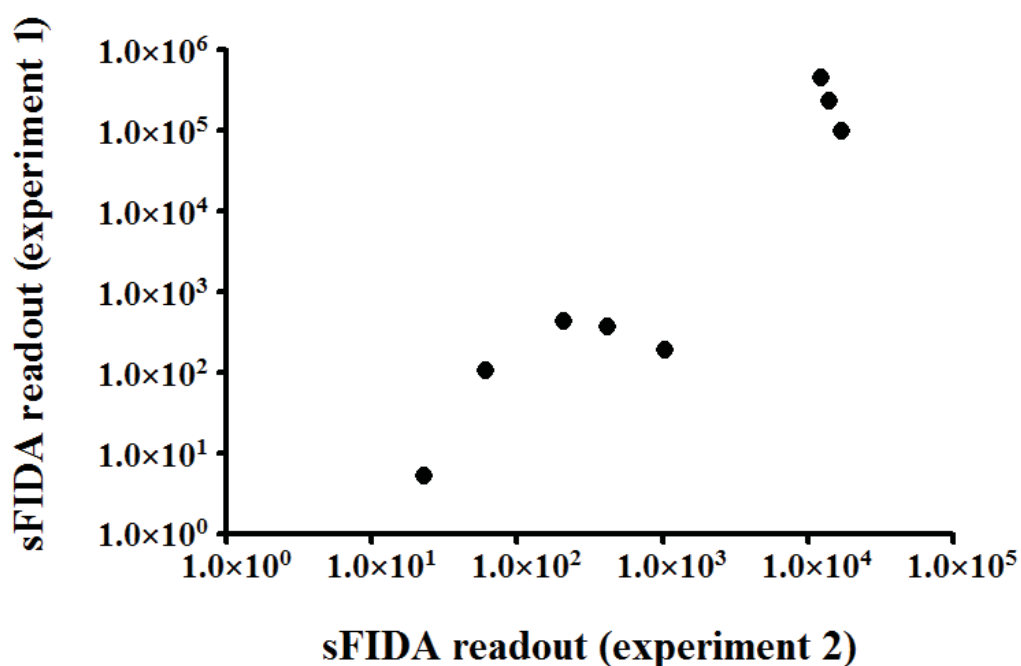
Figure 3-11: Correlation analysis of the sFIDA readout values from the two experiments

The sFIDA readout values of the same 8 samples from the two experiments were analyzed for their correlation. The sFIDA readout values from multiple images of the same sample were averaged and the mean sFIDA readout values were plotted. Each data point represents one individual sample. Spearman correlation was performed (two-tailed $p = 0.0218$, Spearman $r = 0.8095$).

The change in the concentration of CSF Aβ1-42 has been connected to AD in previous studies. Figure 3-12 shows the Aβ1-42 concentrations of the 19 CSF samples measured in experiment 2. Each data point represents one individual sample. The Aβ1-42 concentration of the control group is significantly higher than that of the MCI and AD groups. But there is no significant difference between the MCI and AD groups (student's t-test).

Figure 3-12: Aβ1-42 concentration of the 19 CSF samples

Aβ1-42 concentration of 10 control, 6 MCI and 3 AD samples. Each data point represents one individual sample. Information on the Aβ1-42 concentration was provided by Prof. Piotr Lewczuk, Universitätsklinikum Erlangen. The student's t-test (95% confidence interval) was used for the statistical analysis. "ns" means no significant difference.

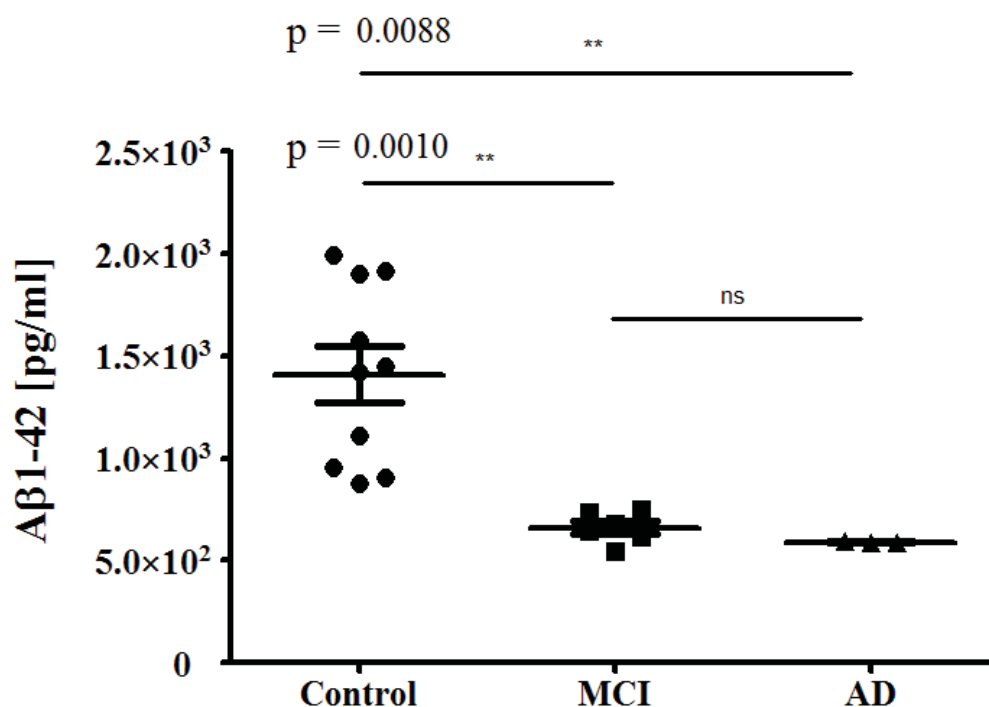The correlation between the sFIDA readout value and the Aβ1-42 level of the 19 CSF samples was explored. As shown in Figure 3-13, there was a significant correlation between the Aβ1-42 concentration and the sFIDA readout value from experiment 2 (two-tailed p = 0.0079, Spearman r = 0.5895). This suggests that the Aβ oligomer level of those CSF samples is positively correlated to the Aβ1-42 concentration.
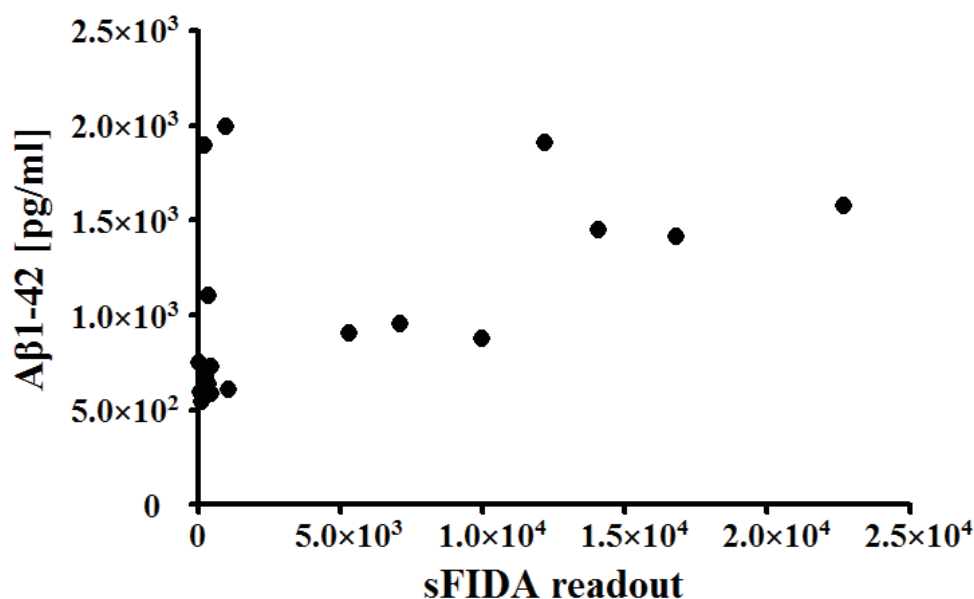
Figure 3-13: Correlation analysis of the sFIDA readout value and Aβ1-42 concentration

sFIDA readout data and Aβ1-42 concentration of 10 control, 6 MCI and 3 AD samples. The sFIDA readout values from multiple images of the same sample were averaged and the mean sFIDA readout values were plotted. Each data point represents one individual sample. Information on the Aβ1-42 concentration was provided by Prof. Piotr Lewczuk, Universitätsklinikum Erlangen. Spearman correlation was performed (two-tailed p = 0.0079, Spearman r = 0.5895).

The human CSF samples from Biochemed could be distinguished by the control and AD groups. In general, the samples of control group showed lower signals compared to those of the AD group. However, the human CSF samples from Universitätsklinikum Erlangen could be hardly distinguished between the control, MCI and AD groups. In general, the samples of the control group showed higher signals than those of the MCI and AD groups. The human CSF samples from different sources did not show the same relationship between the control and AD types. This

might be due to the different handling during the collection and storage of the samples.

However, when the same samples are measured in repeating experiments, if they show distinct relationship between the control and AD types, it is necessary to figure out whether it is due to the changes in the samples or the variation of the assay. To compare one measurement to another, it is essential to have a quality control and a reference standard for sFIDA assay. The quality control should inspect the glass surface treated by sFIDA protocol, especially the capture antibody on the surface as it is responsible for immobilizing the target in the sample. The reference standard should show concentration dependency in a consistent manner.

3.3 Quality control of the capture antibody

The capture antibodies immobilized on the glass surface are responsible for recognizing and binding the target (e.g. Aβ peptides) in the samples. Therefore the quality of the capture antibody is crucial for sFIDA assay to function. Fluorescence labeled capture antibody (see 2.2.1) was used to explore the homogeneity of the capture antibody on the surface. A series of concentrations of the capture antibody were applied to the surface and Aβ aggregates were applied as target. The fluorescence signals of the fluorescence labeled capture antibody and fluorescence labeled detection antibodies were detected. The binding capacity of the antibody to the dextran surface was studied by a series of mixtures of fluorescence labeled antibody and non-labeled antibody (see 2.2.8).

3.3.1 Qualitative analysis of the capture antibody surface

In order to explore the homogeneity of the capture antibodies on the surface, monoclonal antibody NAB228 was fluorescence labeled with Alexa Fluor 546 (see 2.2.1) and 0.03 µg/µl of NAB228-Alexa Fluor 546 was directly cross-linked to the activated dextran layer according to sFIDA protocol (see 2.2.4). To test whether the fluorescence labeled capture antibody could immobilize Aβ peptides, 0.5 µM synthetic Aβ aggregates were applied as the target. The target was probed by

44

detection antibodies 6E10-Alexa Fluor 488 and NAB228-Alexa Fluor 647 and PBS without Aβ aggregates was used as control. The fluorescence signals were then measured by confocal LSM. The images from each fluorescence channel and the merge are shown in Figure 3-14, which demonstrates the distribution of capture surface was homogenous for both PBS control and Aβ aggregates. In the case of Aβ aggregates, the signals from the two fluorescence channels corresponding to the detection antibodies show colocalized bright particles, while no significant signals could be detected in the PBS control. The fluorescence labeled NAB228-Alexa Fluor 546 visually demonstrated the quality of the capture antibodies on the surface.
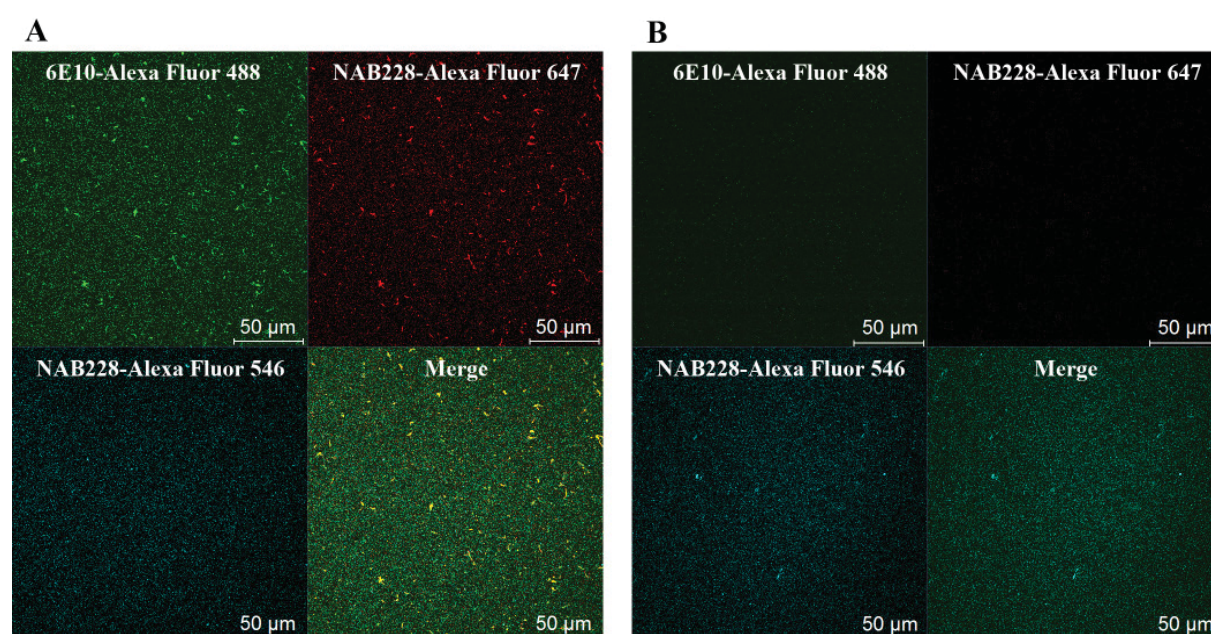
Figure 3-14: The visualized distribution of fluorescence-labeled capture antibody

The Aβ aggregates were immobilized on the surface via fluorescence-labeled capture antibody NAB228-Alexa Fluor 546. 6E10-Alexa Fluor 488 and NAB228-Alexa Fluor 647 were applied as detection antibodies. The merge of the three fluorescence channels was also shown. (A) 0.5 µM Aβ aggregates (B) PBS control without Aβ. Scale bar is 50 µm.

3.3.2 The concentration gradient of capture antibody

It is important to find out how many capture antibodies can bind to the dextran surface so that the amount of capture antibodies applied to the dextran surface is neither too low nor too high. To explore this binding capacity of the capture antibody

to the surface, a series of concentration gradient of capture antibody were used. Aβ aggregates were applied as target and were probed by detection antibodies 6E10-Alexa Fluor 488 and NAB228-Alexa Fluor 647. PBS without Aβ aggregates was used as control. The fluorescence signals were then measured by confocal LSM.

Figure 3-15 shows that the sFIDA readout from 0.5 µM Aβ aggregates is dependent on the concentration of the capture antibody NAB228 within the range of 0.01, 0.03 and 0.05 µg/µl. However, at a higher concentration of 0.10 µg/µl the sFIDA readout did not increase in comparison to the concentrations of 0.05 µg/µl. This could indicate that the concentration for the binding of capture antibody NAB228 to reach saturation was not higher than 0.05 µg/µl.
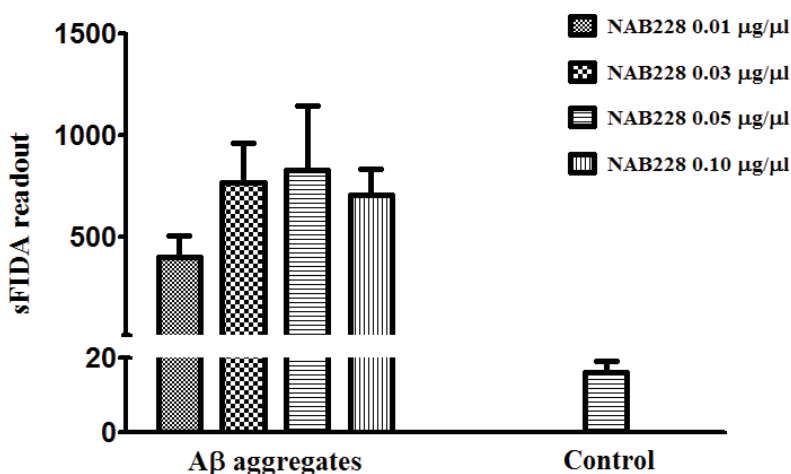
Figure 3-15: Aβ aggregates binding under concentration gradient of capture antibody

The binding to Aβ aggregates (0.5 µM) of capture antibody NAB228 at different concentrations (0.01, 0.03, 0.05 and 0.10 µg/µl) was tested with sFIDA. The concentration of capture antibody of the control was 0.03 µg/µl. The detection antibodies were 6E10-Alexa Fluor 488 and NAB228-Alexa Fluor 647. The sFIDA readout values from multiple images of the same sample were averaged and the mean sFIDA readout values were plotted. Error bars were shown as the SEM.

3.3.3 Capture antibody competition

Another approach to quantitatively explore the binding capacity of the capture antibody to the surface was the capture antibody competition experiment. A mixture

of two components, the fluorescence labeled antibody 6E10-Alexa Fluor 488 (Table 2-3) and the unlabeled antibody NAB228 (Table 2-3), was applied to the glass surface. 6E10-Alexa Fluor 488 and NAB228 would compete to bind to the surface. The protocol for this experiment included the standard steps of the sFIDA protocol (see 2.2.4) till the step of capture antibody incubation, followed by an additional step of 1% sodium dodecyl sulfate (SDS) washing. The SDS washing could remove unspecific bound antibodies, leaving only covalently bound ones. The fluorescence signals were then measured by TIRF microscopy.

The binding of 6E10-Alexa Fluor 488 was indicated by the fluoresce signal given by Alexa Fluor 488. The fluorescence intensity was defined by Equation 3-1. The percentage of fluorescence intensity was introduced in Equation 3-2 to evaluate the changes of fluorescence intensity.

Equation 3-1: Calculation of the fluorescence intensity (I)

$$\text{Fluorescence Intensity} \, (I) = \sum_{i=0}^{i_{max}} (i \times n_i)$$

i	value of the grayscale
i_{max}	the maximum value of the grayscale
n_i	pixel count at the grayscale of i

Equation 3-2: Calculation of the percentage of fluorescence intensity

$$\text{Fluorescence Intensity} \, \% = \frac{I_c - I_{PBS}}{I_0 - I_{PBS}}$$

I_c	Fluorescence intensity (I) of the NAB228 concentration c µg/µl
I_0	Fluorescence intensity (I) of the NAB228 concentration 0 µg/µl
I_{PBS}	Fluorescence intensity (I) of PBS

As the concentration of non-labeled antibody increased in the mixture, the fluorescence signal from 6E10-Alexa Fluor 488 decreased (Figure 3-16 and Figure 3-17). The reason is that the two kinds of antibodies competed for the binding sites on the surface. One phase exponential decay equation model was used to fit the data set. Determined by the fitting, the half maximum of the covalent binding of the

6E10-Alexa Fluor 488 to the surface corresponds to approximately 0.0066 µg/µl of NAB228. This suggested that approximately 0.0066 µg/µl of capture antibody would be enough for covalent binding to the dextran surface. Therefore the concentration of the capture antibody in the sFIDA protocol has been adjusted from 0.03 µg/µl to 0.01 µg/µl.
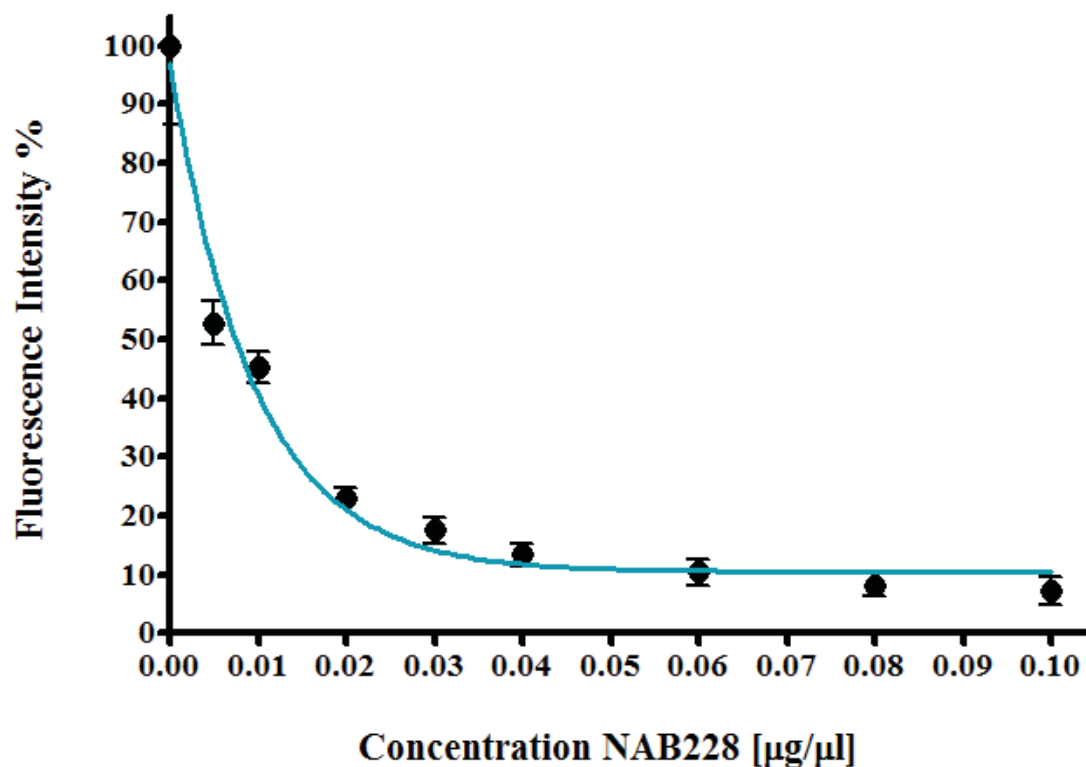
Figure 3-16: Analysis of the binding competition of the capture antibodies

In the mixture of antibodies, the concentration of 6E10-Alexa Fluor 488 was constant at 0.001 µg/µl, while the concentration of NAB228 ranged from 0 to 0.10 µg/µl. Fluorescence Intensity % indicates the percentage of the fluorescence intensity of each sample divided by the maximum fluorescence intensity. Error bars were shown as the SEM. The data set was fitted by one phase exponential decay equation model.
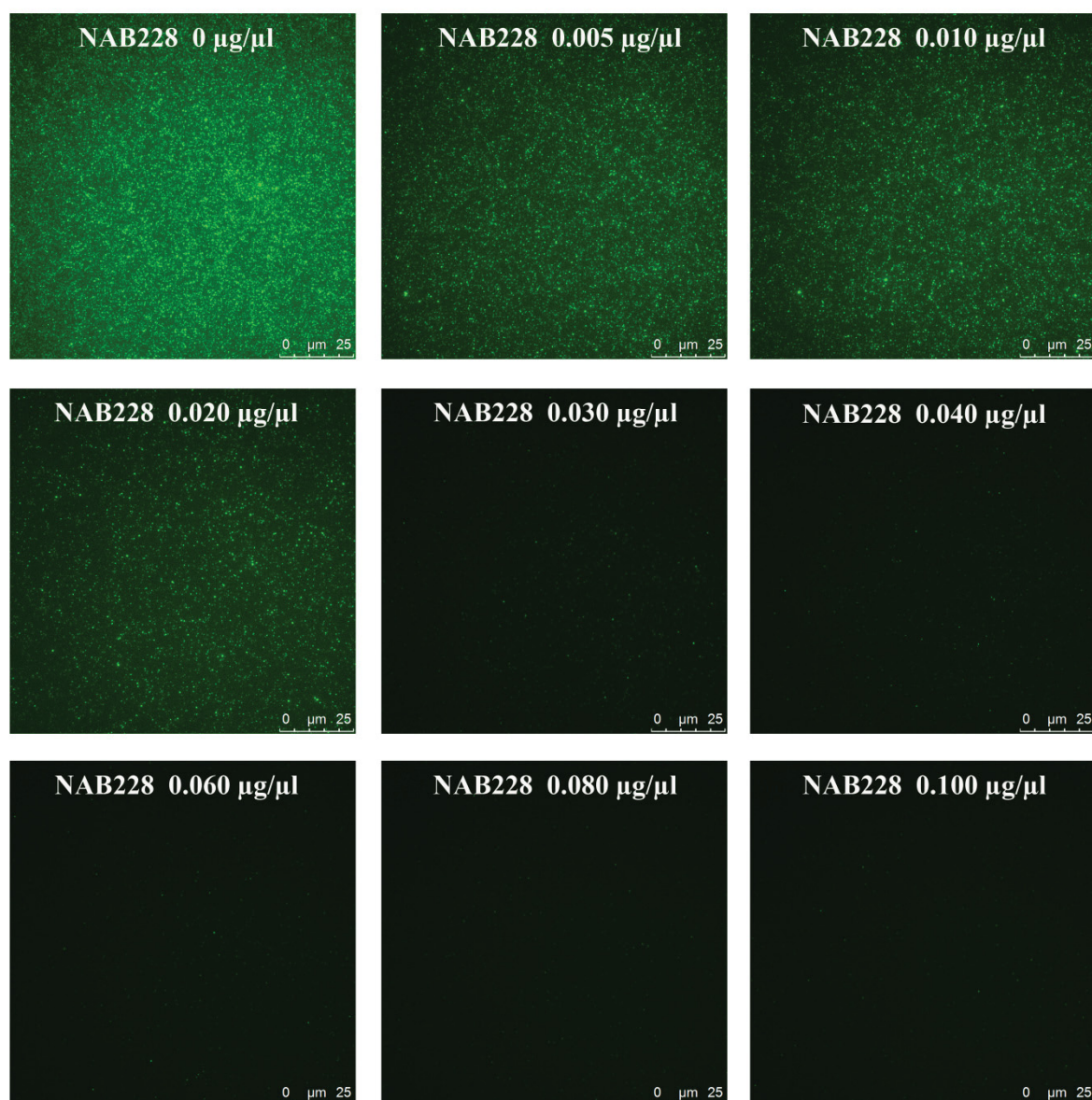
Figure 3-17: TIRF images of the binding competition of the capture antibodies

The images were taken by TIRF microscopy. Each image represents one single scanning area of a multiple-position scanning. A series of mixture of 6E10-Alexa Fluor 488 at 0.001 µg/µl and NAB228 ranging from 0 to 0.100 µg/µl were immobilized on the glass surface. The concentration of NAB228 of each mixture is indicated. Scale bar is 25 µm.

3.4 Exploration of MAP as a reference standard

It is essential to establish a reliable reference system for sFIDA, so that the measurement-to-measurement signal variation can be calibrated. For this end the MAP molecules were developed to be used as a reference standard. The multiple antigenic peptide (MAP) system was initially developed to improve the weak immunogenicity of subunit peptide vaccines (Tam, 1988). MAP molecules are constructed on a non-immunogenic lysine-based dendritic scaffold. The α- and side chain ε-amino groups make lysine suitable for creating branching structure which multiple units of antigenic peptides bind to. Compared with small antigenic peptides, the MAP molecules are more resistant against enzymatic degradation and enhance the immune recognition. The MAP molecules have shown the potential in vaccine development (Fujita and Taguchi, 2011). Besides, the MAP molecules have also been utilized as a calibration standard for single antibody sandwich ELISA (SAS-ELISA) system (Kasai et al., 2012). In this study, 16- or 32-branched MAP were designed by multiplying 4- or 8-branched MAP. 16MAP and 32MAP were then constructed, purified and tested in sFIDA assay.

3.4.1 Construction and purification of MAP

The 4MAP or 8MAP molecule, which comprises multiple N-terminus epitopes (amino acids 1-11 of Aβ1-42) linked to a branching scaffold, was synthesized (Table 2-4). Via its biotinylated scaffold 4MAP and 8MAP are able to bind to streptavidin molecules. Each tetrameric streptavidin molecule can bind up to four units of 4MAP or 8MAP respectively. The formation of 16MAP and 32MAP is depicted in Figure 3-18.
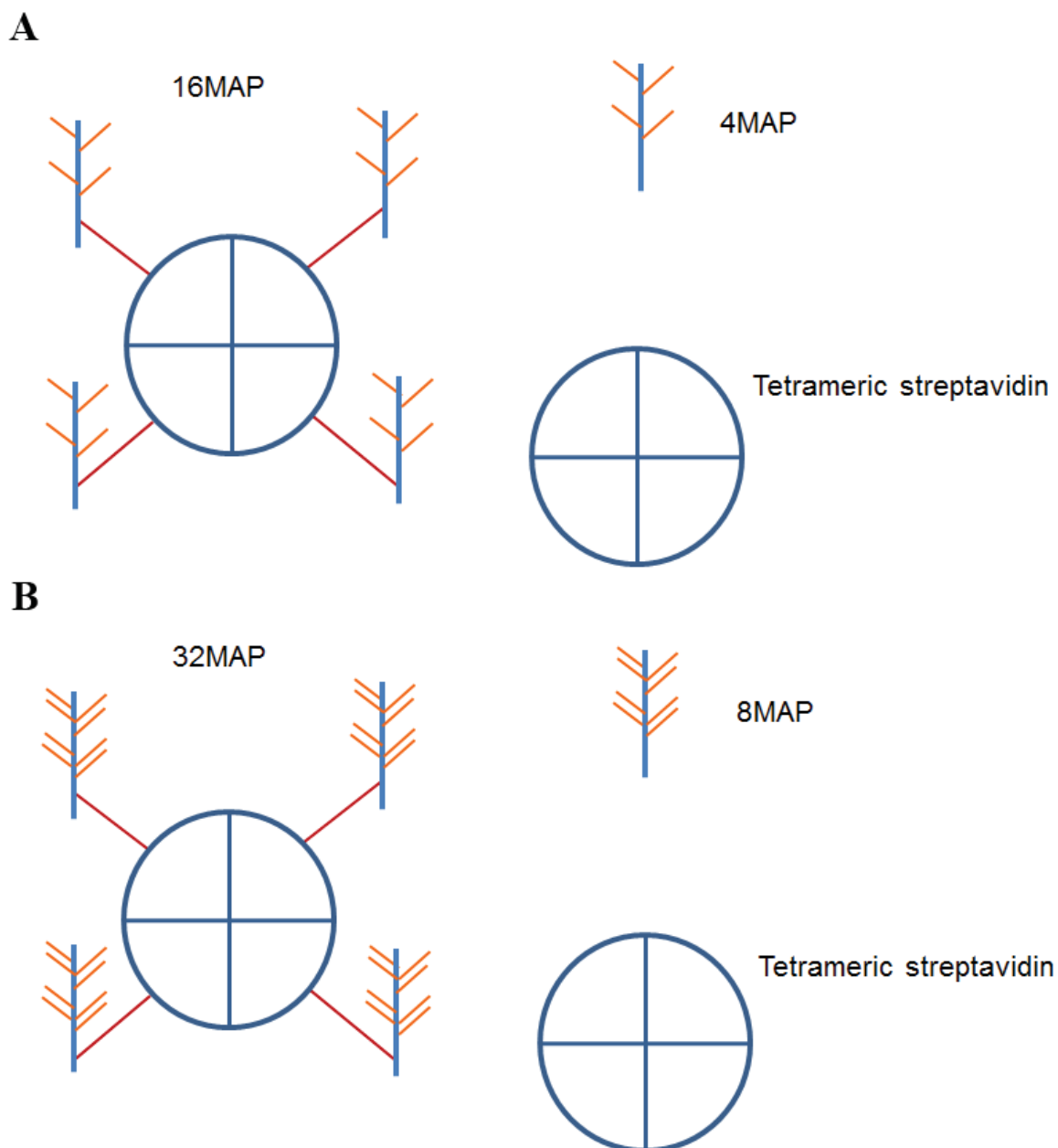
Figure 3-18: Formation of 16MAP and 32MAP

One tetrameric streptavidin molecule can bind up to four 4MAP or 8MAP molecules. Streptavidin homo-tetramers have an extraordinarily high affinity for biotin with a dissociation constant (Kd) on the order of ≈10−14 mol/L (Green, 1975).

16MAP and 32MAP were prepared as described (see 2.2.2). After the binding of 4MAP/8MAP with streptavidin, the reaction mixture was applied to the SEC column (Table 2-9). The 16MAP fraction eluted at a retention volume of 13.41 ml. The 32MAP fraction eluted at a retention volume of 12.77 ml (Figure 3-19). As determined by UV absorption, the concentrations of the peak fraction of 16MAP and 32MAP were 0.68 µM and 0.12 µM respectively.
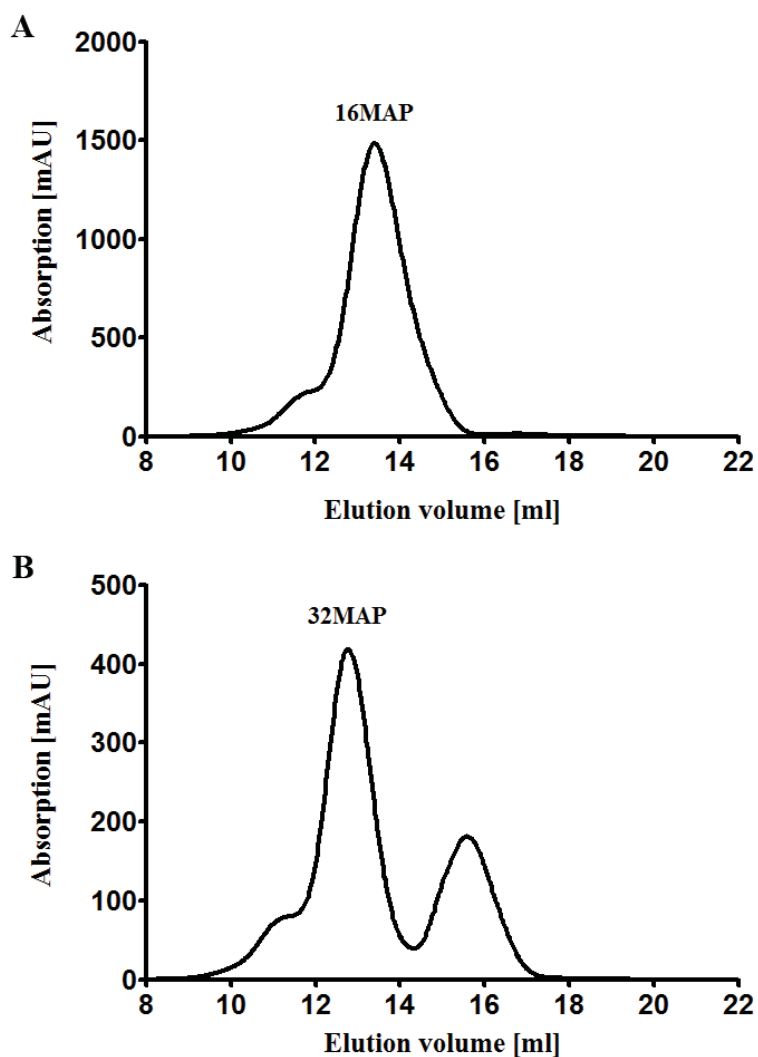
Figure 3-19: Purification of 16MAP and 32MAP

16MAP (A) and 32MAP (B) were purified by SEC. The absorption (mAU: milli absorption unit) was detected at 214 nm and plotted vs. the elution volume. A Superdex 200 10/300 GL column was used to perform the purification. With the flow rate of 0.5 ml/min, 16MAP (91 kDa) fraction eluted at a retention volume of 13.41 ml and 32MAP (113 kDa) fraction eluted at retention volume of 12.77 ml.

3.4.2 sFIDA measurements of 16MAP and 32MAP

16MAP and 32MAP molecules prepared from SEC were diluted in PBS in a series of concentrations and then measured by sFIDA. They were immobilized on a ZAT microtiter plate according to the sFIDA protocol (see 2.2.4).

In the pilot experiment, 32MAP was applied in a range from 80 pM to 640 pM (Figure 3-20). The fluorescence signals were then measured by confocal LSM. The sFIDA readout in the mentioned concentration range was concentration dependent.
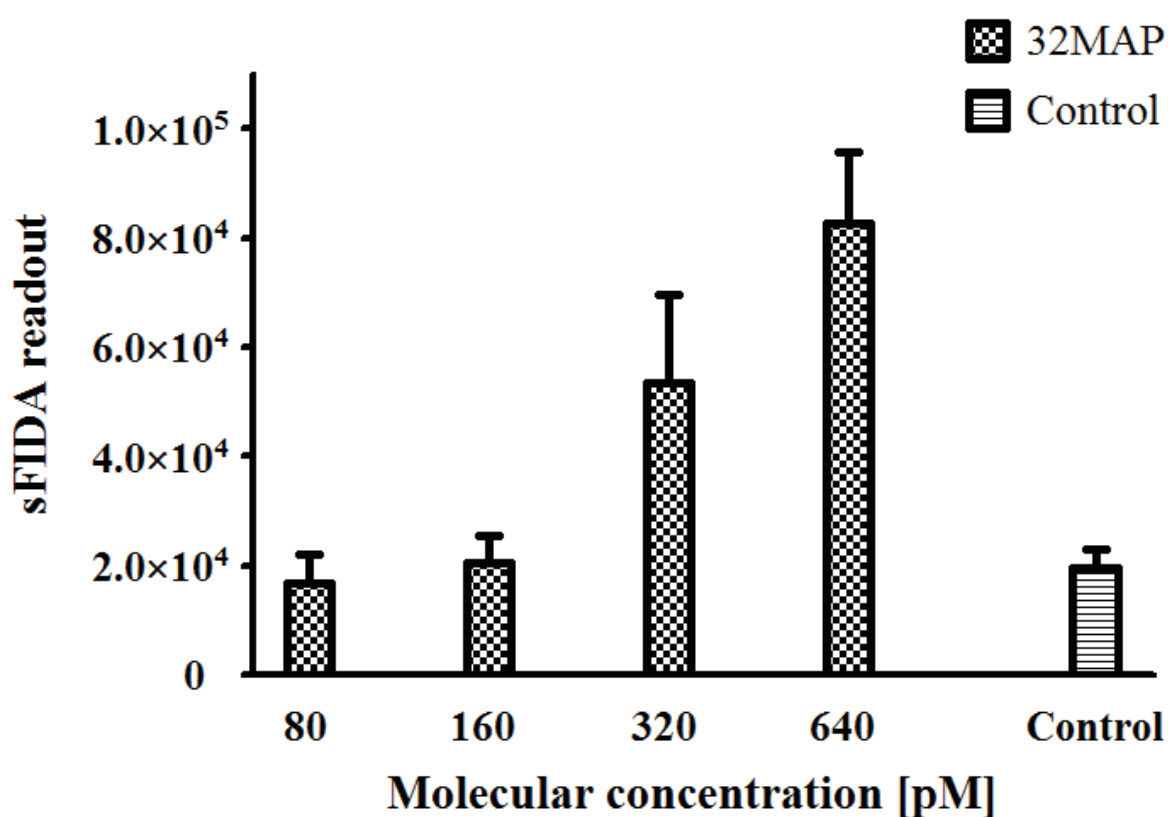
Figure 3-20: Detection of 32MAP by sFIDA

32MAP in a concentration series ranging from 80 pM to 640 pM were detected by sFIDA. PBS was applied as the buffer control. 6E10-Alexa Fluor 488 and IC16-Alexa Fluor 647 were applied as detection antibodies. Error bars are shown as the SEM.

53

In the following experiment, lower concentration of 16MAP and 32MAP were tested by sFIDA. The fluorescence signals were then measured by TIRF microscopy. Figure 3-21 shows the sFIDA readout obtained from 16MAP and 32MAP ranging from 1 pM to 100 pM. It can be observed that the signals from 32MAP were consistently higher than those of 16MAP probably due to the higher content of epitopes in 32MAP. The concentration-dependence of the signals derived from both 16MAP and 32MAP reached a limit at 10 pM. The concentration of Aβ in biological fluid (e.g. human CSF) is usually in the range of low picomolar or even sub-picomolar, therefore the detection limit of 10 pM for 16MAP and 32MAP may not be sensitive enough to calibrate the sFIDA assay for measuring human CSF samples.
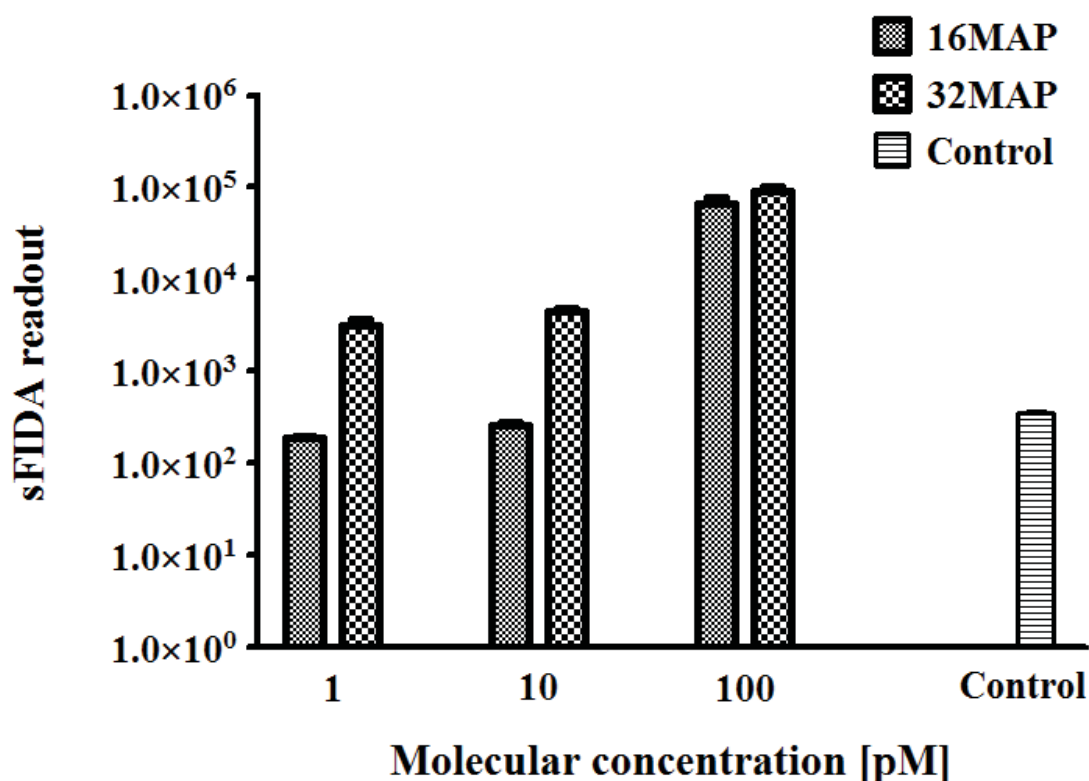
Figure 3-21: Detection of 16MAP and 32MAP by sFIDA

16MAP and 32MAP in a concentration series ranging from 1 pM to 100 pM were detected by sFIDA. PBS was applied as the buffer control. 6E10-ATTO 488 and IC16-Alexa Fluor 633 were applied as detection antibodies. Error bars are shown as the SEM.

4 Discussion

Alzheimer's disease (AD) is a progressive neurodegenerative disease with the characteristic symptom of cognitive impairment. AD affects mostly the people in the age group above 65. As the world's population is rapidly ageing, the number of AD cases would witness a rapid increase. At present, the only definitive diagnosis is through the *post mortem* autopsy. There is no cure for AD so far. Therefore, a robust diagnosis is needed to identify the disease at its early stage and to evaluate the therapeutic effects of potential drugs. AD pathology is featured by the amyloid plaques and the neurofibrillary tangles (NFTs). The amyloid plaques are mostly composed of amyloid-β (Aβ) peptides, while the NFTs are formed by aggregated tau proteins. Though there are various diagnostic approaches such as cognitive test, standard medical tests and brain imaging (Jack et al., 2011), they only show limited accuracy. Currently the efforts on early detection of AD depend on biomarkers which indicate the biological or pathological processes of AD. Some AD biomarkers have already shown the potential for the diagnosis in the preclinical stage of AD (Jack and Holtzman, 2013). In a hypothetical model, CSF Aβ1-42 is suggested to be the biomarker which emerges ahead of other biomarkers in the progression of AD (Jack et al., 2013). The decreased CSF Aβ1-42 level could be related to the Aβ aggregation and deposition in the brain. The soluble Aβ oligomers have been proposed to account for the neurotoxicity (Glabe, 2006). Several methods have been available to detect Aβ oligomers, although the limitation is that they could only provide the information of the overall concentration of Aβ oligomers. Further development of an assay that is capable of detecting Aβ oligomers on the single molecule level would provide more sensitive detection as well as more comprehensive information such as the shape and size of the Aβ oligomers.

4.1 Establishment of sFIDA on TIRF microscopy

Several biomarkers have been proposed for the diagnosis of AD (Jack et al., 2013). The outstanding advantage of CSF Aβ1-42 is that evidence suggested that CSF Aβ1-42 emerges ahead of other AD biomarker such as tau in the AD progression. The decreased CSF Aβ1-42 level could be caused by the Aβ aggregation and deposition in the brain. And the soluble Aβ oligomers have been proposed to account for the neurotoxicity (Glabe, 2006) and play a central role in the AD pathogenesis. Therefore the reliable detection of Aβ aggregates could provide early and direct information about the AD development. Several techniques have been developed to investigate the Aβ oligomer level. Those methods include immunoblotting (Tomic et al., 2009), enzyme-linked immunosorbent assay (ELISA) (LeVine, 2004) and a nanoparticle-based bio-barcode assay (Georganopoulou et al., 2005). One common disadvantage of those methods is that they can only provide the overall concentration of Aβ oligomers within the sample, but without the information such as the shape, size and composition of the Aβ oligomers. The technique called surface-based-fluorescence intensity distribution analysis (sFIDA) was developed to detect single Aβ oligomer particles.

sFIDA was initially established on fluorescence correlation spectroscopy (FCS) to detect single prion protein particles (Birkmann et al., 2006). Then the assay was adapted to confocal laser scanning microscope (LSM) for detecting Aβ aggregates (Funke et al., 2007). sFIDA assay could specifically detect the Aβ oligomers but not the Aβ monomers in the samples. This relates the result of the assay to the AD pathology, because previous evidences supported that the oligomeric form of Aβ rather than the monomeric form of Aβ accounts for the neurotoxicity (Glabe, 2006). Compared to the very small detection volume of FCS, the measurement by LSM could cover a larger proportion of the targets in the sample. Besides, LSM could provide further information about the Aβ aggregates such as the shape and the size. total internal reflection fluorescence (TIRF) microscopy provides high-resolution imaging as LSM does, moreover TIRF microscopy enables much faster imaging than LSM thanks to its EM-CCD detector. Firstly this benefit has increased the throughput of the assay. Secondly it is possible to measure each sample in triplicate wells. Another benefit of TIRF microscopy is that only the fluorophores in a range of approximately some hundred nanometers above the glass-media interface are

excited. This can generate images with a high signal-to-noise ratio with hardly any background fluorescence from out-of-focus planes (source: MicroscopyU, http://www.microscopyu.com/). This penetration depth of the excitation is suitable to detect the fluorescence labeled detection antibodies on the glass surface in the sFIDA assay. And with the Leica software operating the microscope, the multi-well measurement can be done in an automated manner which saves a lot of time for the operator. The customized software sFIDAta developed in the institute has greatly facilitated the data analysis.

4.2 Human CSF sample from different sources performed differently in sFIDA assay

The cerebrospinal fluid (CSF) system circulates nutrients to and removes waste products from the brain. Recent studies suggested that the CSF contains more than just nutrients and waste, but also actively released substances from the brain which could indicate the changes in brain activity (Veening and Barendregt, 2010). The soluble Aβ oligomers have been proposed to account for the neurotoxicity (Glabe, 2006) and play a central role in the AD pathogenesis. The CSF Aβ oligomers could act as an indicator of the disease status of AD. By measuring of the CSF Aβ oligomers, sFIDA has shown promising result in identifying different types of human CSF samples (Wang-Dietrich et al., 2013). However, the CSF samples from different sources are usually not collected and stored under the same condition. This could affect the components of the CSF samples and thus the CSF samples from different sources could show distinct relationship between different types of CSF samples. Therefore it is a challenge to measure various sample pools by sFIDA. Human CSF samples from Biochemed (Table 2-5) and Prof. Piotr Lewczuk in Universitätsklinikum Erlangen (Table 2-6) were measured and analyzed by sFIDA.

However, these two sources of human CSF samples showed distinct relationship between the control group and AD group in sFIDA assay. There is a significant difference in the sFIDA readout between the control group and AD group from Biochemed samples. In general the control samples demonstrated lower sFIDA readout values than the AD samples. This suggests that the Aβ oligomer level of the

control samples is lower than that of the AD samples. Among the AD samples, the highest Aβ oligomer level can be two times higher than the lowest (see 3.2.1). The observation is consistent with the previous studies which reported that the Aβ oligomer levels were higher in AD patients than that in the non-demented individuals (Pitschke et al., 1998; Wang-Dietrich et al., 2013). Besides, in the study of the amyloid-β-derived diffusible ligand (ADDL) in CSF, the concentrations of ADDL were lower in control group than those in the AD group, while variation among the individuals in the AD group was observed (Georganopoulou et al., 2005).

However, the CSF samples from Universitätsklinikum Erlangen did not show the same pattern. Two independent experiments were performed for those samples. In both experiments most of the control samples demonstrated higher sFIDA readout values than AD and MCI samples, though except for the control samples and MCI samples in experiment 2, there is no significant distinction between any of the different CSF types (see 3.2.2). The sFIDA readout values of the same samples from the two experiments showed significant positive correlation, which suggested the experiments were reproducible. The different patterns observed in the human CSF samples from different sources might be caused by the different handling during the collection and storage of the samples.

The CSF samples from Universitätsklinikum Erlangen showed decreased Aβ1-42 level in the MCI and AD groups compared to the control group. This is consistent with the previous reports which demonstrated a decrease of CSF Aβ1-42 in AD. And this decrease could be caused by the Aβ aggregation in the brain and/or CSF, or the unbalance in the metabolism of amyloid precursor protein (APP) and Aβ (Andreasen and Blennow, 2002). In this study, Aβ oligomer level was specifically measured by sFIDA. This could help monitor the Aβ oligomers level in CSF in parallel to the changes in the level of CSF Aβ1-42. And the relationship between the Aβ oligomers level and the Aβ1-42 level could be analyzed.

4.3 The quality of capture antibody on the surface could be assessed

In the sFIDA protocol, the capture antibodies on the glass surface are responsible for specifically immobilizing the Aβ in the sample, which are then detected by fluorescence labeled detection antibodies. The quality of the capture antibodies on the surface determines the performance of the whole assay. The primary consideration is whether the distribution of the capture antibodies is homogeneous. If not, the immobilization of the Aβ on the surface might be uneven. If the scanning area covers the region where Aβ is uneven immobilized, the images would bring greater variance to the analysis. In this study, capture antibody was fluorescence labeled with a fluorescence dye distinct from those of the two fluorescence labeled detection antibodies. With the fluorescence signal from the labeled capture antibody, the homogeneity of the surface was shown. And it could provide important information such as whether the inhomogeneity in the fluorescence signals indicating the Aβ target is related to the distribution of the capture antibody. This strategy enabled the acquirement of the fluorescence signal of the capture antibody in parallel to the detection of target. This provides a direct qualitative assessment of the capture antibody on the surface.

Another consideration for the capture antibody is what concentration should be applied in the sFIDA protocol. If the concentration is too low, the capture antibody would not be able to utilize the available binding sites on the surface. If the concentration is too high, the high density of the capture antibody on the surface might make some of the epitopes unavailable due to the spatial hindrance. In the previous work, the concentration of the capture antibodies was set to 0.03 µg/µl (Wang-Dietrich et al., 2013). In the concentration gradient experiment of this study, the capture antibody showed a concentration dependency in the range of 0.01-0.05 µg/µl. This is in accordance to the previous work. However, the following capture antibody competition experiment, in which the noncovalent bound capture antibodies were removed, suggested a more optimal concentration close to 0.01 µg/µl. Therefore the concentration of capture antibody was modified from 0.03 µg/µl to 0.01 µg/µl in the sFIDA protocol.

4.4 MAP molecules showed limited potential as a reference standard

One of the difficulties to quantitatively analyze the sFIDA measurement was the lack of a reference system to calibrate the variation from one measurement to another. The key to the system is a reference standard which can be applied to sFIDA protocol and detected as a target. The reference standard should provide concentration dependent output in a stable and reproducible manner. For this purpose the multiple antigenic peptide (MAP) was explored for its potential as a reference standard in this work. The MAP system was originally developed to improve the weak immunogenicity of subunit peptide vaccines (Tam, 1988). A MAP molecule contains multiple units of antigenic peptides on a non-immunogenic lysine-based dendritic scaffold. The MAP molecules enhance the resistance against enzymatic degradation and the immune recognition, in comparison with the small antigenic peptides. In previous work the MAP molecules have been established as a calibration standard for single antibody sandwich ELISA (SAS-ELISA) system (Kasai et al., 2012).

In this work, the amino acids 1-11 of the human amyloid-β protein were chosen to be the antigenic peptide and 4 and 8 units of this antigenic peptide were bound to a lysine scaffold respectively. Because of the difficulty of synthesizing MAP molecules with epitopes number such as 16 or even 32, 16MAP and 32MAP were then constructed by binding biotinylated 4MAP or 8MAP to a streptavidin core via biotin-streptavidin interaction. In sFIDA assay, the sFIDA readout values of 32MAP were consistently higher than that of 16MAP in a series of concentrations. This is as expected because 32MAP has the doubled amount of epitopes as the 16MAP. However, the concentration dependence of the sFIDA readout of either 16MAP or 32MAP was limited to about 10 pM. As the Aβ oligomer level in human CSF is expected to be at low picomolar or even sub-picomolar, the current detection limit of 16MAP and 32MAP may not be sensitive enough for the calibration of the sFIDA assay when measuring human CSF samples. There are several possible reasons. Firstly, the conformation of the 16MAP and 32MAP may not be favorable for the recognition by the detection antibodies. Secondly, the multiple epitopes of 16MAP and 32MAP might be mostly occupied by the capture antibodies, leaving limited

number of epitopes available for the detection antibodies, therefore affecting the detection of the MAP molecule. To overcome this problem, one way is to re-design the branching structure of the MAP molecules to provide more spatial flexibility and availability for antibody recognition. If the detection limit can be achieved to sub-picomolar range, the MAP could be applied to calibrate the sFIDA assay for measuring CSF samples.

5 Summary

Alzheimer's disease (AD) is a neurodegenerative disease, which accounts for the most common dementia in the age group above 65. So far the only definitive diagnosis can be established by post mortem autopsy. However, a diagnosis in the preclinical stage would be essential for early intervention of the disease. Since Amyloid-β (Aβ) in its diffusible oligomeric isoform is a key player in AD pathology, it represents a promising biomarker candidate, which can be detected in body fluids. Surface-based fluorescence intensity distribution analysis (sFIDA) is a technology to detect single Aβ aggregates. Briefly, Aβ aggregates are immobilized on a capture surface and loaded with fluorescent antibody probes followed by fluorescence microscopy.

In this work, sFIDA was adapted to total internal reflection fluorescence microscopy, which enables fast and automated multi-well imaging. sFIDA measurements of human cerebrospinal fluid (CSF) samples from a commercial source revealed elevated Aβ oligomers level in the AD group in comparison with the control group. This result is in accordance with previous observations and supports that the CSF Aβ oligomer can be used as a biomarker for AD. However, other CSF samples from a clinical source showed no significant difference in the Aβ oligomer levels between control and AD group, which might be due to different handling during the collection and storage of the samples.

In the course of this work single steps in the sFIDA were analyzed and optimized with special focus on the capture antibody surface. The use of fluorescence-labeled capture antibodies demonstrated the homogeneity of the capture antibody distribution on the glass surface. Competition analysis between fluorescence-labeled capture antibody and non-labeled capture antibody revealed the actual amount of capture antibody that was cross-linked to the glass surface. The multiple antigenic peptide (MAP) molecules 16MAP and 32MAP showed some potential to be used as reference standard to calibrate sFIDA assay, though the limit of detection has yet to be optimized.

6 Zusammenfassung

Die Alzheimersche Demenz (AD) ist eine neurodegenerative Krankheit und die häufigste Form von Demenz ab dem 65sten Lebensjahr. Bisher ist eine eindeutige Diagnose nur durch eine Autopsie post mortem möglich. Eine sichere Diagnose in der präklinischen Phase wäre aber von hoher Bedeutung, um früh in den Krankheitsverlauf eingreifen zu können. Amyloid β (Aβ) spielt in seiner löslichen oligomeren Isoform eine entscheidende Rolle in der AD Pathogenese und stellt somit einen vielversprechenden Biomarker in verschiedenen Körperflüssigkeiten dar. Die oberflächenbasierte Fluoreszenz-Verteilungsanalyse (sFIDA) ist eine Technik zur Detektion von Aβ-Oligomeren. Aß Aggregate werden auf einer mit Fänger-Antikörpern beschichteten Oberfläche immobilisiert, mit fluoreszierenden Antikörpern versetzt und anschließend durch konfokale Mikroskopie vermessen.

In dieser Arbeit wurde sFIDA auf interne Totalreflexionsfluoreszenz Mikroskopie angepasst, wodurch eine schnelle und automatische Bildaufnahme ermöglich wird. sFIDA Messungen von käuflich erworbenen Liquor Proben zeigten eine erhöhte Konzentration an Aβ-Oligomeren in der AD-Gruppe im Vergleich zur Kontroll-Gruppe. Dieses Ergebnis stimmt mit vorherigen Beobachtungen überein und unterstützt die Annahme, dass Aβ-Oligomere in Liquor als Biomarker für AD dienen können. Liquor-Proben klinischer Herkunft zeigten hingegen keinen signifikanten Unterschied in der Aβ-Oligomer-Konzentration von Kontroll- und AD-Proben, was durch unterschiedliche Arbeitsweisen bei der Probenentnahme und der Lagerung der Proben zu erklären sein könnte.

Im Rahmen dieser Arbeit wurden verschiedene Schritte des sFIDA analysiert und optimiert, wobei der Fokus auf der Antikörperbeschichtung der Glasoberfläche lag. Durch die Verwendung von Fluoreszenz-markierten Fänger-Antikörpern konnte eine homogene Fluoreszenzverteilung auf der Oberfläche gezeigt werden. Anhand der Kompetition von Fluoreszenz-markiertem und nicht markiertem Antikörper wurde die Menge an kovalent immobilisiertem Antikörper ermittelt. Schließlich konnte für sog. multiple antigenic peptides (MAP) 16MAP und 32MAP nahegelegt werden, dass diese als potenzielle Referenzmoleküle zur Kalibrierung des sFIDA eingesetzt werden können, wobei das Detektionslimit optimiert werden sollte.

Abbreviations

Aβ	amyloid-β
AβpGlu	pyroglutamate amyloid-β
AD	Alzheimer's disease
ADDL	amyloid-β-derived diffusible ligand
APP	amyloid precursor protein
AU	absorption unit
BSA	bovine serum albumin
CMD	carboxymethyl dextran
CSF	cerebrospinal fluid
Da	dalton
ddH_2O	double-distilled water
DMSO	dimethyl sulfoxide
EDC	N-(3-dimethyl-aminopropyl)-N'-ethylcarbodiimide hydrochloride
ELISA	enzyme-linked immunosorbent assay
fM	femtomolar
h	hour
HCl	hydrochloric acid
KCl	potassium chloride
kDa	kilodalton
KH_2PO_4	monopotassium phosphate
L	liter
LSM	laser scanning microscope
M	molar
ml	milliliter
mM	millimolar
MCI	mild cognitive impairment
min	minute
NHS	N-hydroxysuccinimide
nM	nanomolar
nm	nanometer
NaCl	sodium chloride

PBS	phosphate buffered saline
pM	picomolar
SDS	sodium dodecyl sulfate
SEC	size exclusion chromatography
sFIDA	surface-based-fluorescence intensity distribution analysis
TBS	tris-buffered saline
TBST	tris-buffered saline-tween
TIRF	total internal reflection fluorescence
UV	ultraviolet
v/v	volume per volume
w/v	weight per volume
µM	micromolar
µl	microliter

Reference

Alzheimer, A., 1907, About a peculiar disease of the cerebral cortex: Centralblatt für Nervenheilkunde Psychiatrie, v. 30, p. 177-179.

Andreasen, N., and K. Blennow, 2002, Beta-amyloid (Abeta) protein in cerebrospinal fluid as a biomarker for Alzheimer's disease: Peptides, v. 23, p. 1205-14.

Baker, H. F., R. M. Ridley, L. W. Duchen, T. J. Crow, and C. J. Bruton, 1993, Evidence for the experimental transmission of cerebral beta-amyloidosis to primates: Int J Exp Pathol, v. 74, p. 441-54.

Ballard, C., S. Gauthier, A. Corbett, C. Brayne, D. Aarsland, and E. Jones, 2011, Alzheimer's disease: Lancet, v. 377, p. 1019-31.

Bannach, O., E. Birkmann, E. Reinartz, K. E. Jaeger, J. P. Langeveld, R. G. Rohwer, L. Gregori, L. A. Terry, D. Willbold, and D. Riesner, 2012, Detection of prion protein particles in blood plasma of scrapie infected sheep: PLoS One, v. 7, p. e36620.

Baruch-Suchodolsky, R., and B. Fischer, 2009, Abeta40, either soluble or aggregated, is a remarkably potent antioxidant in cell-free oxidative systems: Biochemistry, v. 48, p. 4354-70.

Bird, T. D., 1993, Alzheimer Disease Overview, *in* R. A. Pagon, M. P. Adam, H. H. Ardinger, T. D. Bird, C. R. Dolan, C. T. Fong, R. J. H. Smith, and K. Stephens, eds., GeneReviews(R): Seattle (WA).

Birkmann, E., F. Henke, N. Weinmann, C. Dumpitak, M. Groschup, A. Funke, D. Willbold, and D. Riesner, 2007, Counting of single prion particles bound to a capture-antibody surface (surface-FIDA): Vet Microbiol, v. 123, p. 294-304.

Birkmann, E., O. Schafer, N. Weinmann, C. Dumpitak, M. Beekes, R. Jackman, L. Thorne, and D. Riesner, 2006, Detection of prion particles in samples of BSE and scrapie by fluorescence correlation spectroscopy without proteinase K digestion: Biol Chem, v. 387, p. 95-102.

Bitan, G., M. D. Kirkitadze, A. Lomakin, S. S. Vollers, G. B. Benedek, and D. B. Teplow, 2003, Amyloid beta -protein (Abeta) assembly: Abeta 40 and Abeta 42 oligomerize through distinct pathways: Proc Natl Acad Sci U S A, v. 100, p. 330-5.

Braak, H., K. Del Tredici, U. Rub, R. A. de Vos, E. N. Jansen Steur, and E. Braak, 2003, Staging of brain pathology related to sporadic Parkinson's disease: Neurobiol Aging, v. 24, p. 197-211.

Brookmeyer, R., S. Gray, and C. Kawas, 1998, Projections of Alzheimer's disease in the United States and the public health impact of delaying disease onset: Am J Public Health, v. 88, p. 1337-42.

Brookmeyer, R., E. Johnson, K. Ziegler-Graham, and H. M. Arrighi, 2007, Forecasting the global burden of Alzheimer's disease: Alzheimers Dement, v. 3, p. 186-91.

Burns, A., and S. Iliffe, 2009, Alzheimer's disease: BMJ, v. 338, p. b158.

Caughey, B., G. S. Baron, B. Chesebro, and M. Jeffrey, 2009, Getting a grip on prions: oligomers, amyloids, and pathological membrane interactions: Annu Rev Biochem, v. 78, p. 177-204.

Dickerson, B. C., and D. A. Wolk, 2012, MRI cortical thickness biomarker predicts AD-like CSF and cognitive decline in normal adults: Neurology, v. 78, p. 84-90.

Drzezga, A., 2010, Amyloid-plaque imaging in early and differential diagnosis of dementia: Ann Nucl Med, v. 24, p. 55-66.

Duyckaerts, C., 2011, Tau pathology in children and young adults: can you still be unconditionally baptist?: Acta Neuropathol, v. 121, p. 145-7.

Ebner, A., P. Hinterdorfer, and H. J. Gruber, 2007, Comparison of different aminofunctionalization strategies for attachment of single antibodies to AFM cantilevers: Ultramicroscopy, v. 107, p. 922-7.

Fujita, Y., and H. Taguchi, 2011, Current status of multiple antigen-presenting peptide vaccine systems: Application of organic and inorganic nanoparticles: Chem Cent J, v. 5, p. 48.

Funke, S. A., E. Birkmann, F. Henke, P. Gortz, C. Lange-Asschenfeldt, D. Riesner, and D. Willbold, 2007, Single particle detection of Abeta aggregates associated with Alzheimer's disease: Biochem Biophys Res Commun, v. 364, p. 902-7.

Gandy, S., 2005, The role of cerebral amyloid beta accumulation in common forms of Alzheimer disease: J Clin Invest, v. 115, p. 1121-9.

Georganopoulou, D. G., L. Chang, J. M. Nam, C. S. Thaxton, E. J. Mufson, W. L. Klein, and C. A. Mirkin, 2005, Nanoparticle-based detection in cerebral spinal fluid of a soluble pathogenic biomarker for Alzheimer's disease: Proc Natl Acad Sci U S A, v. 102, p. 2273-6.

Glabe, C. G., 2006, Common mechanisms of amyloid oligomer pathogenesis in degenerative disease: Neurobiol Aging, v. 27, p. 570-5.

Glenner, G. G., and C. W. Wong, 1984a, Alzheimer's disease and Down's syndrome: sharing of a unique cerebrovascular amyloid fibril protein: Biochem Biophys Res Commun, v. 122, p. 1131-5.

Glenner, G. G., and C. W. Wong, 1984b, Alzheimer's disease: initial report of the purification and characterization of a novel cerebrovascular amyloid protein: Biochem Biophys Res Commun, v. 120, p. 885-90.

Goedert, M., W. J. Strittmatter, and A. D. Roses, 1994, Alzheimer's disease. Risky apolipoprotein in brain: Nature, v. 372, p. 45-6.

Green, N. M., 1975, Avidin: Adv Protein Chem, v. 29, p. 85-133.

Grundke-Iqbal, I., K. Iqbal, Y. C. Tung, M. Quinlan, H. M. Wisniewski, and L. I. Binder, 1986, Abnormal phosphorylation of the microtubule-associated protein tau (tau) in Alzheimer cytoskeletal pathology: Proc Natl Acad Sci U S A, v. 83, p. 4913-7.

Hardy, J., and D. J. Selkoe, 2002, The amyloid hypothesis of Alzheimer's disease: progress and problems on the road to therapeutics: Science, v. 297, p. 353-6.

Henkel, A. W., P. S. Dittrich, T. W. Groemer, E. A. Lemke, J. Klingauf, H. W. Klafki, P. Lewczuk, H. Esselmann, P. Schwille, J. Kornhuber, and J. Wiltfang, 2007, Immune complexes of auto-antibodies against A beta 1-42 peptides patrol cerebrospinal fluid of non-Alzheimer's patients: Mol Psychiatry, v. 12, p. 601-10.

Hernandez, F., and J. Avila, 2007, Tauopathies: Cell Mol Life Sci, v. 64, p. 2219-33.

Igbavboa, U., G. Y. Sun, G. A. Weisman, Y. He, and W. G. Wood, 2009, Amyloid beta-protein stimulates trafficking of cholesterol and caveolin-1 from the plasma membrane to the Golgi complex in mouse primary astrocytes: Neuroscience, v. 162, p. 328-38.

Iwatsubo, T., A. Odaka, N. Suzuki, H. Mizusawa, N. Nukina, and Y. Ihara, 1994, Visualization of A beta 42(43) and A beta 40 in senile plaques with end-specific A beta monoclonals: evidence that an initially deposited species is A beta 42(43): Neuron, v. 13, p. 45-53.

Jack, C. R., Jr., M. S. Albert, D. S. Knopman, G. M. McKhann, R. A. Sperling, M. C. Carrillo, B. Thies, and C. H. Phelps, 2011, Introduction to the recommendations from the National Institute on Aging-Alzheimer's Association workgroups on diagnostic guidelines for Alzheimer's disease: Alzheimers Dement, v. 7, p. 257-62.

Jack, C. R., Jr., and D. M. Holtzman, 2013, Biomarker modeling of Alzheimer's disease: Neuron, v. 80, p. 1347-58.

Jack, C. R., Jr., D. S. Knopman, W. J. Jagust, R. C. Petersen, M. W. Weiner, P. S. Aisen, L. M. Shaw, P. Vemuri, H. J. Wiste, S. D. Weigand, T. G. Lesnick, V. S. Pankratz, M. C. Donohue, and J. Q. Trojanowski, 2013, Tracking pathophysiological processes in Alzheimer's disease: an updated hypothetical model of dynamic biomarkers: Lancet Neurol, v. 12, p. 207-16.

Jagust, W. J., D. Bandy, K. Chen, N. L. Foster, S. M. Landau, C. A. Mathis, J. C. Price, E. M. Reiman, D. Skovronsky, and R. A. Koeppe, 2010, The Alzheimer's Disease Neuroimaging Initiative positron emission tomography core: Alzheimers Dement, v. 6, p. 221-9.

Jucker, M., 2010, The benefits and limitations of animal models for translational research in neurodegenerative diseases: Nat Med, v. 16, p. 1210-4.

Kang, J., H. G. Lemaire, A. Unterbeck, J. M. Salbaum, C. L. Masters, K. H. Grzeschik, G. Multhaup, K. Beyreuther, and B. Muller-Hill, 1987, The precursor of Alzheimer's disease amyloid A4 protein resembles a cell-surface receptor: Nature, v. 325, p. 733-6.

Kasai, T., T. Tokuda, M. Taylor, M. Nakagawa, and D. Allsop, 2012, Utilization of a multiple antigenic peptide as a calibration standard in the BAN50 single antibody sandwich ELISA for Abeta oligomers: Biochem Biophys Res Commun, v. 422, p. 375-80.

LaFerla, F. M., K. N. Green, and S. Oddo, 2007, Intracellular amyloid-beta in Alzheimer's disease: Nat Rev Neurosci, v. 8, p. 499-509.

LeVine, H., 3rd, 2004, Alzheimer's beta-peptide oligomer formation at physiologic concentrations: Anal Biochem, v. 335, p. 81-90.

Lewczuk, P., H. Esselmann, M. Meyer, V. Wollscheid, M. Neumann, M. Otto, J. M. Maler, E. Ruther, J. Kornhuber, and J. Wiltfang, 2003, The amyloid-beta (Abeta) peptide pattern in cerebrospinal fluid in Alzheimer's disease: evidence of a novel carboxyterminally elongated Abeta peptide: Rapid Commun Mass Spectrom, v. 17, p. 1291-6.

Masters, C. L., G. Simms, N. A. Weinman, G. Multhaup, B. L. McDonald, and K. Beyreuther, 1985, Amyloid plaque core protein in Alzheimer disease and Down syndrome: Proc Natl Acad Sci U S A, v. 82, p. 4245-9.

Mattsson, N., H. Zetterberg, O. Hansson, N. Andreasen, L. Parnetti, M. Jonsson, S. K. Herukka, W. M. van der Flier, M. A. Blankenstein, M. Ewers, K. Rich, E. Kaiser, M. Verbeek, M. Tsolaki, E. Mulugeta, E. Rosen, D. Aarsland, P. J. Visser, J. Schroder, J. Marcusson, M. de Leon, H. Hampel, P. Scheltens, T. Pirttila, A. Wallin, M. E. Jonhagen, L. Minthon, B. Winblad, and K. Blennow, 2009, CSF biomarkers and incipient Alzheimer disease in patients with mild cognitive impairment: JAMA, v. 302, p. 385-93.

Molsa, P. K., R. J. Marttila, and U. K. Rinne, 1986, Survival and cause of death in Alzheimer's disease and multi-infarct dementia: Acta Neurol Scand, v. 74, p. 103-7.

Nakagawa, T., H. Zhu, N. Morishima, E. Li, J. Xu, B. A. Yankner, and J. Yuan, 2000, Caspase-12 mediates endoplasmic-reticulum-specific apoptosis and cytotoxicity by amyloid-beta: Nature, v. 403, p. 98-103.

Pitschke, M., R. Prior, M. Haupt, and D. Riesner, 1998, Detection of single amyloid beta-protein aggregates in the cerebrospinal fluid of Alzheimer's patients by fluorescence correlation spectroscopy: Nat Med, v. 4, p. 832-4.

Price, J. L., D. W. McKeel, Jr., V. D. Buckles, C. M. Roe, C. Xiong, M. Grundman, L. A. Hansen, R. C. Petersen, J. E. Parisi, D. W. Dickson, C. D. Smith, D. G. Davis, F. A. Schmitt, W. R. Markesbery, J. Kaye, R. Kurlan, C. Hulette, B. F. Kurland, R. Higdon, W. Kukull, and J. C. Morris, 2009, Neuropathology of nondemented aging: presumptive evidence for preclinical Alzheimer disease: Neurobiol Aging, v. 30, p. 1026-36.

Priller, C., T. Bauer, G. Mitteregger, B. Krebs, H. A. Kretzschmar, and J. Herms, 2006, Synapse formation and function is modulated by the amyloid precursor protein: J Neurosci, v. 26, p. 7212-21.

Santos, A. N., S. Torkler, D. Nowak, C. Schlittig, M. Goerdes, T. Lauber, L. Trischmann, M. Schaupp, M. Penz, F. W. Tiller, and G. Bohm, 2007, Detection of amyloid-beta oligomers in human cerebrospinal fluid by flow cytometry and fluorescence resonance energy transfer: J Alzheimers Dis, v. 11, p. 117-25.

Schilling, S., S. Kohlmann, C. Bauscher, R. Sedlmeier, B. Koch, R. Eichentopf, A. Becker, H. Cynis, T. Hoffmann, S. Berg, E. J. Freyse, S. von Horsten, S. Rossner, S. Graubner, and H. U. Demuth, 2011, Glutaminyl cyclase knock-out mice exhibit slight hypothyroidism but no hypogonadism: implications for enzyme function and drug development: J Biol Chem, v. 286, p. 14199-208.

Schlenzig, D., S. Manhart, Y. Cinar, M. Kleinschmidt, G. Hause, D. Willbold, S. A. Funke, S. Schilling, and H. U. Demuth, 2009, Pyroglutamate formation influences solubility and amyloidogenicity of amyloid peptides: Biochemistry, v. 48, p. 7072-8.

Seubert, P., C. Vigo-Pelfrey, F. Esch, M. Lee, H. Dovey, D. Davis, S. Sinha, M. Schlossmacher, J. Whaley, C. Swindlehurst, and et al., 1992, Isolation and quantification of soluble Alzheimer's beta-peptide from biological fluids: Nature, v. 359, p. 325-7.

Sgourakis, N. G., Y. Yan, S. A. McCallum, C. Wang, and A. E. Garcia, 2007, The Alzheimer's peptides Abeta40 and 42 adopt distinct conformations in water: a combined MD / NMR study: J Mol Biol, v. 368, p. 1448-57.

Shankar, G. M., S. Li, T. H. Mehta, A. Garcia-Munoz, N. E. Shepardson, I. Smith, F. M. Brett, M. A. Farrell, M. J. Rowan, C. A. Lemere, C. M. Regan, D. M. Walsh, B. L. Sabatini, and D. J. Selkoe, 2008, Amyloid-beta protein dimers isolated directly from Alzheimer's brains impair synaptic plasticity and memory: Nat Med, v. 14, p. 837-42.

Shoji, M., T. E. Golde, J. Ghiso, T. T. Cheung, S. Estus, L. M. Shaffer, X. D. Cai, D. M. McKay, R. Tintner, B. Frangione, and et al., 1992, Production of the Alzheimer amyloid beta protein by normal proteolytic processing: Science, v. 258, p. 126-9.

Small, S. A., and K. Duff, 2008, Linking Abeta and tau in late-onset Alzheimer's disease: a dual pathway hypothesis: Neuron, v. 60, p. 534-42.

Tabaton, M., X. Zhu, G. Perry, M. A. Smith, and L. Giliberto, 2010, Signaling effect of amyloid-beta(42) on the processing of AbetaPP: Exp Neurol, v. 221, p. 18-25.

Tam, J. P., 1988, Synthetic peptide vaccine design: synthesis and properties of a high-density multiple antigenic peptide system: Proc Natl Acad Sci U S A, v. 85, p. 5409-13.

Thal, D. R., U. Rub, M. Orantes, and H. Braak, 2002, Phases of A beta-deposition in the human brain and its relevance for the development of AD: Neurology, v. 58, p. 1791-800.

Tomic, J. L., A. Pensalfini, E. Head, and C. G. Glabe, 2009, Soluble fibrillar oligomer levels are elevated in Alzheimer's disease brain and correlate with cognitive dysfunction: Neurobiol Dis, v. 35, p. 352-8.

Veening, J. G., and H. P. Barendregt, 2010, The regulation of brain states by neuroactive substances distributed via the cerebrospinal fluid; a review: Cerebrospinal Fluid Res, v. 7, p. 1.

Visser, P. J., F. Verhey, D. L. Knol, P. Scheltens, L. O. Wahlund, Y. Freund-Levi, M. Tsolaki, L. Minthon, A. K. Wallin, H. Hampel, K. Burger, T. Pirttila, H. Soininen, M. O. Rikkert, M. M. Verbeek, L. Spiru, and K. Blennow, 2009, Prevalence and prognostic value of CSF markers of Alzheimer's disease pathology in patients with subjective cognitive impairment or mild cognitive impairment in the DESCRIPA study: a prospective cohort study: Lancet Neurol, v. 8, p. 619-27.

Wang-Dietrich, L., S. A. Funke, K. Kuhbach, K. Wang, A. Besmehn, S. Willbold, Y. Cinar, O. Bannach, E. Birkmann, and D. Willbold, 2013, The amyloid-beta oligomer count in cerebrospinal fluid is a biomarker for Alzheimer's disease: J Alzheimers Dis, v. 34, p. 985-94.

Wenk, G. L., 2003, Neuropathologic changes in Alzheimer's disease: J Clin Psychiatry, v. 64 Suppl 9, p. 7-10.

Wimo, A., and M. Prince, 2011, World Alzheimer Report 2010: The Global Economic Impact of Dementia, Alzheimer's Disease International.

Wong, P. C., H. Cai, D. R. Borchelt, and D. L. Price, 2002, Genetically engineered mouse models of neurodegenerative diseases: Nat Neurosci, v. 5, p. 633-9.

Younkin, S. G., 1998, The role of A beta 42 in Alzheimer's disease: J Physiol Paris, v. 92, p. 289-92.

Eidesstattliche Erklärung

Ich versichere an Eides Statt, dass die Dissertation von mir selbständig und ohne unzulässige fremde Hilfe unter Beachtung der "Grundsätze zur Sicherung guter wissenschaftlicher Praxis an der Heinrich-Heine-Universität Düsseldorf" erstellt worden ist.

Jülich, den

Kun Wang

Acknowledgement

I would like to thank my supervisor, Prof. Dr. Dieter Willbold, for giving me this opportunity to participate in this project. I have learned a lot from his critical thinking, enthusiasm and patience for science.

I would like to thank Prof. Dr. Georg Groth for reviewing my dissertation.

I would like to express my gratitude to Dr. Oliver Bannach for the insightful discussions and mentoring of my PhD thesis.

I would like to thank all sFIDA group members, Dr. Andreas Kulawik, Katja Kühbach, Maren Hülsemann, Yvonne Herrmann, Kateryna Kravchenko, Dr. Eva Birkmann, Elke Reinartz, Dr. Tuyen Bujnicki, Dr. Christian Zafiu, Christina Linnartz, Loreano Peters, Johannes Willbold for their helpful suggestions and encouraging discussions of my work.

Thanks to Dr. Susanne Aileen Funke and Dr. Lei Wang-Dietrich who has helped me a lot on my project.

I thank the cooperation partner Prof. Dr. Piotr Lewczuk from Universitätsklinikum Erlangen for kindly providing the human CSF samples.

I would like to thank Dr. Peixiang Ma and Dr. Yu-Fu Hung for the helpful discussions.

I would like to thank my office mates Stephan Rudolph, Olga Valdau and Christina Möller for the discussions and help.

I thank all members of the Institute of Complex Systems for structure biochemistry (ICS-6).

My apologies to those who I have not mentioned by name, I am indebted to them for the help they offered.

Last but not least, I would thank my family. Only with their persistent love and support can I finish this work.